Taylor & Francis
Taylor & Francis Group

Australian Journal of Earth Sciences

An International Geoscience Journal of the Geological Society of Australia

ISSN: (Print) (Online) Journal homepage: https://www.tandfonline.com/loi/taje20

Zebra rock and other Ediacaran paleosols from Western Australia

G. J. Retallack

To cite this article: G. J. Retallack (2020): Zebra rock and other Ediacaran paleosols from Western Australia, Australian Journal of Earth Sciences, DOI: 10.1080/08120099.2020.1820574

To link to this article: https://doi.org/10.1080/08120099.2020.1820574

Published online: 30 Sep 2020.

AUSTRALIAN JOURNAL OF EARTH SCIENCES
https://doi.org/10.1080/08120099.2020.1820574

Zebra rock and other Ediacaran paleosols from Western Australia

G. J. Retallack

Department of Earth Sciences, University of Oregon, Eugene, USA

ABSTRACT

Zebra rock is an ornamental stone from the early Ediacaran, Ranford Formation, around and in Lake Argyle, south of Kununurra, Western Australia. It has been regarded as a marine clay, liquid crystal, groundwater alteration, unconformity paleosol or product of acid sulfate weathering. This study supports the latter hypothesis and finds modern analogues for its distinctive red banding in mottling of gleyed soils. Other acid sulfate paleosols of desert playas (Gypsids) are also are found in the Ranford Formation, as well as calcareous desert paleosols (Calcids). The megafossil *Palaeopaschnicnus* also found in associated grey shales may have been a chambered protozoan, but *Yangtziramulus* in calcic paleosols is most like a microbial earth lichen. Soil climofunctions are evidence of an arid, cool temperate climate during the early Ediacaran.

KEY POINTS

1. Ornamental stones known as 'zebra rock' are interpreted as Ediacaran gleyed soils.
2. Gypsum desert-rose beds are interpreted as Ediacaran acid sulfate soils (Gypsids).
3. Calcareous nodular loess beds are interpreted as Ediacaran desert soils (Gypsids).

ARTICLE HISTORY
Received 15 June 2020
Accepted 2 September 2020

KEYWORDS
Ranford Formation; Ediacaran; paleosols; *Yangtziramulus*; *Palaeopascichnus*

Introduction

Zebra rock is an ornamental stone unique to northern Western Australia, widely used in jewellery and sculpture. The origin of zebra rock has been regarded as hydrothermal alteration (Kelka *et al.*, 2017; Wallace & Hood, 2018), liesegang banding induced by groundwater (Hobson, 1930), partial leaching of an unconformity paleosol (Trainer, 1931), interbedded marine silt and clay (Geidans, 1981; Larcombe, 1925, 1927), ferronematic banding of a colloidal bed (Mattievich *et al.*, 2003), or a product of acid sulfate soil weathering (Loughnan & Roberts, 1990). The current study aims to adjudicate these alternative origins with additional petrographic and geochemical evidence on zebra rock and other beds in the Ediacaran Ranford Formation and underlying 'cap carbonate' of the Moonlight Valley Tillite near Kununurra, Western Australia (Corkeron, 2007, 2008).

A secondary objective is to understand Ediacaran paleoenvironments and life. Of special interest are problematic Ediacaran megafossils associated with zebra rock, such as *Palaeopascichnus* (Lan & Chen, 2012), *Yangtziramulus* (Shen *et al.*, 2009), and a variety of microbially induced sedimentary structures (Lan & Chen, 2013). Biological affinities and paleoenvironments of Ediacaran megafossils remain puzzling (Retallack & Broz, 2020).

Geological background

Zebra rock forms discontinuous lenses within the shaley Johnny Cake Member of the Ranford Formation in localities from northeast to central Lake Argyle (Figure 1). The underlying sandy, Jarrad Member of the Ranford Formation conformably overlies the 'cap carbonate' of the Moonlight Valley Tillite in Midnight Valley east of Warnum, and at Palm Springs further south (Bao *et al.*, 2012; Corkeron, 2007). The 'cap carbonate' sandstones have been identified as the top 8–10 m of the Midnight Valley Tillite (Kennedy, 1996; Corkeron, 2007), but are very similar to the lowest dolomitic sandstones of the Jarrad Member separated by a poorly exposed interval of shale.

The age of the Ranford Formation is Ediacaran as indicated by fossils of *Palaeopascichnus* (Lan & Chen, 2012). *Yangtziramulus* reported here is another indication of Ediacaran age (Shen *et al.*, 2009). Lithological correlation with other Ediacaran successions in Australia is evidence of early Ediacaran age, below limestones with the stromatolite *Tungussia julia* such as the Egan Formation and Boonall Dolomite of Western Australia (Corkeron, 2007; Grey & Corkeron, 1998), the Julie Limestone of central Australia, and the Wonoka Formation of South Australia (Figure 2). The Ranford Formation also conformably overlies Moonlight Valley Tillite, widely correlated with the terminal Cryogenian, Elatina Glaciation (Corkeron, 2008), commonly

CONTACT G. J. Retallack gregr@uoregon.edu Department of Earth Sciences, University of Oregon, Eugene, OR 97403-1272, USA
Editorial handling: Chris Fergusson

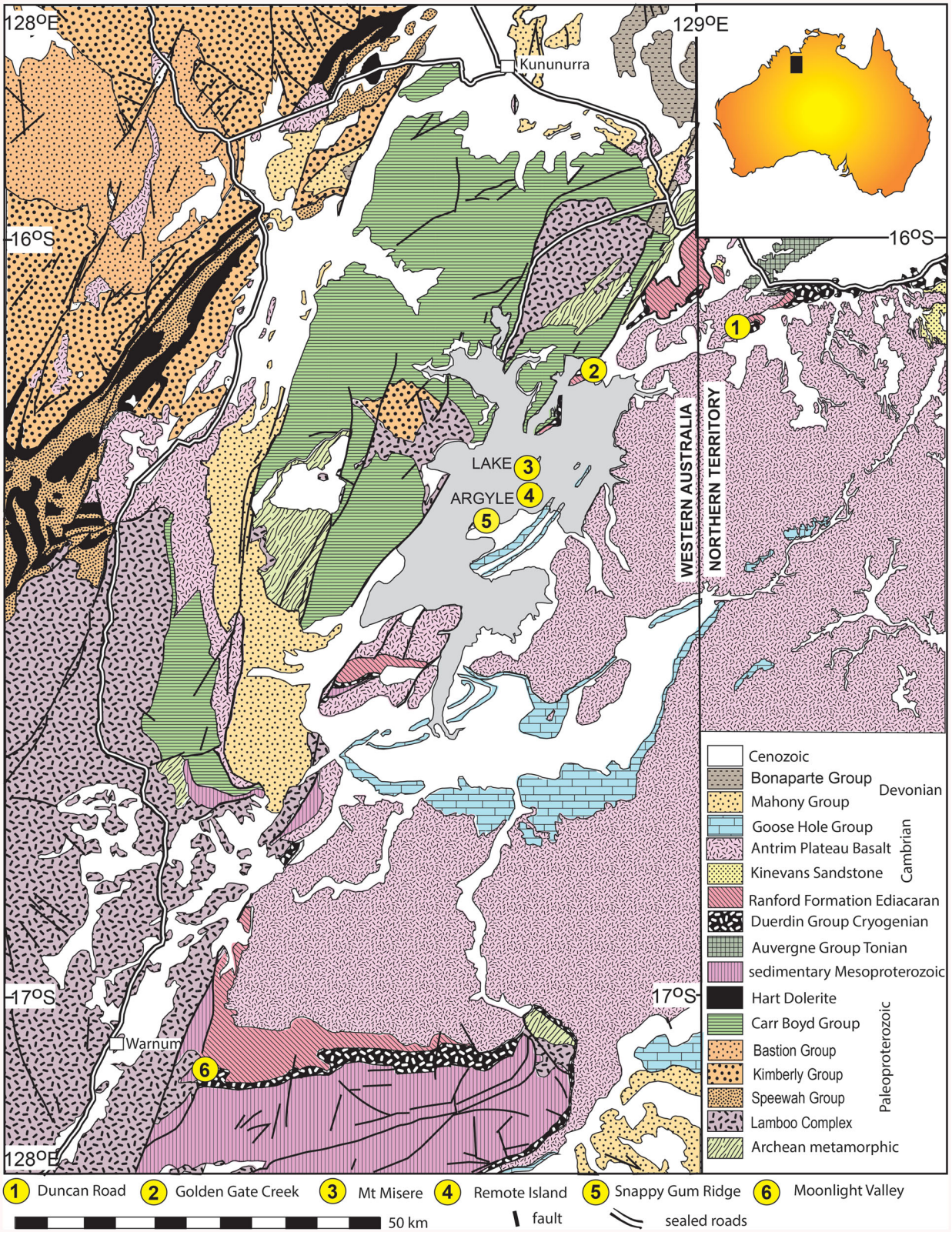

Figure 1. Zebra rock localities around Lake Argyle (1–5) and caprock locality east of Warnum (6), Western Australia (geology after Dow & Gemuts, 1969; Sweet, Mendum, *et al.*, 1974; Sweet, Pontifex, *et al.*, 1974).

misnamed Marinoan (Williams *et al.*, 2008). A negative $\delta^{13}C$ isotopic excursion has been used to justify this correlation (Kennedy, 1996), and this correlation is now supported by a distinctive $\Delta^{17}O$ excursion (Bao *et al.*, 2012). These anomalies define the base of the Ediacaran Period in the type section in South Australia (Knoll *et al.*, 2006), so that the base of the Ediacaran is at the base of the 'cap carbonate' of the Moonlight Valley Tillite rather than 8 m higher

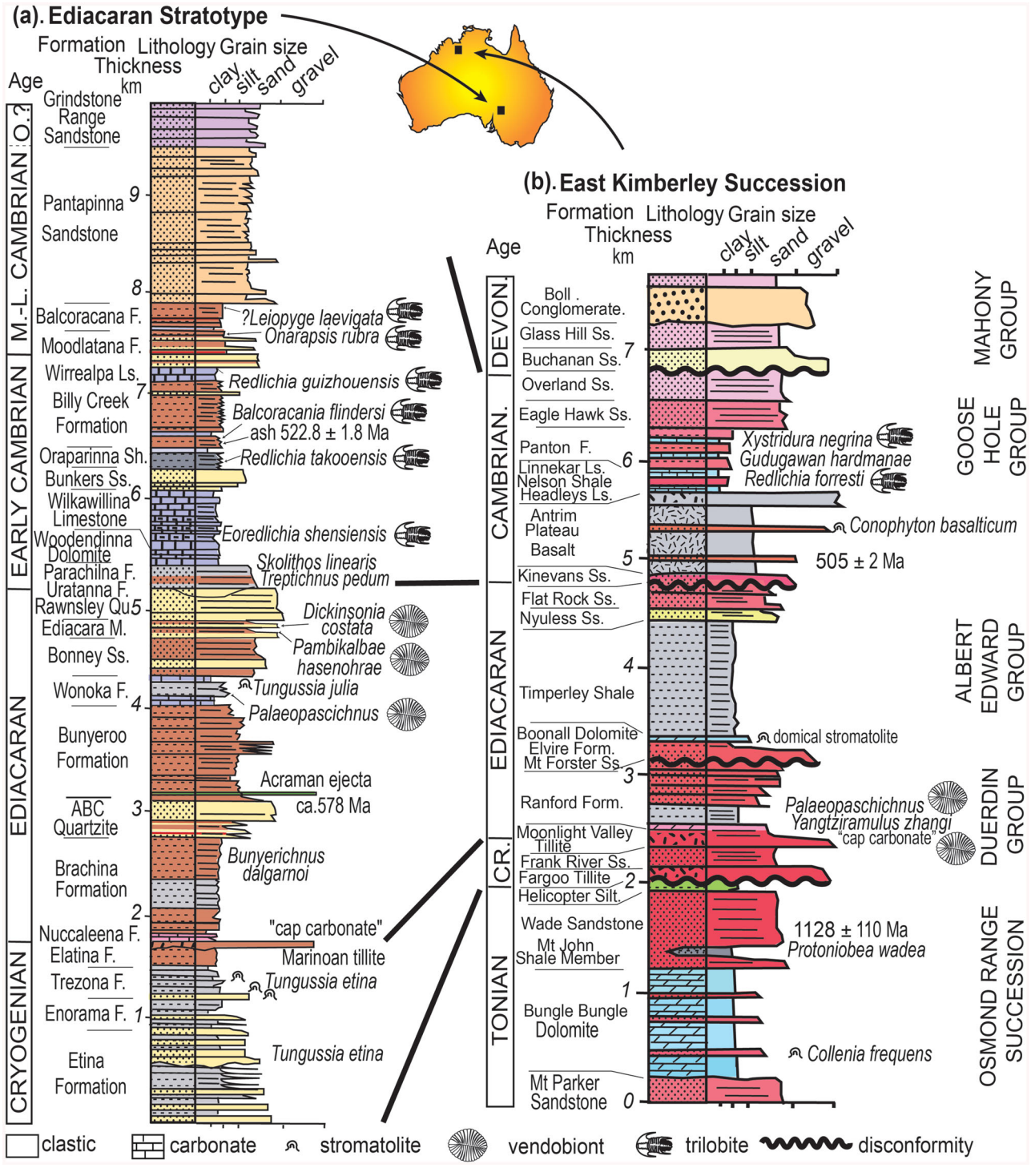

Figure 2. Correlation of the Ranford Formation of Western Australia (after Corkeron, 2007; Grey & Corkeron, 1998; Mory & Beere, 1985; Plumb *et al.*, 1981), with the stratotype Ediacaran succession in South Australia, Australia (after Retallack, 2013).

at the contact with the overlying Ranford Formation (Corkeron, 2007; Kennedy, 1996). An age model using 635 Ma for the base of the cap carbonate, and 567 Ma for top Boonall Dolomite (base Nuccaleena and upper Wonoka of Retallack *et al.*, 2014) gives 635 to 623 Ma for the section measured at Moonlight Valley and 600–599 Ma for short sections measured at Donkey Creek and Duncan Road.

Directions of ice movement in the Moonlight Valley Tillite are from the north (Corkeron, 2008), where tillite forms a thin cap on the Mesoproterozoic (*ca* 1128 Ma) Osmond Range succession (Figure 2). A local Mesoproterozoic source is also indicated by detrital zircons in the Ranford Formation (Lan *et al.*, 2020). The Ranford Formation is disconformably overlain by early Cambrian

Kinevans Sandstone to the north (Sweet, Mendum, *et al.*, 1974; Sweet, Pontifex, *et al.*, 1974), but is overlain by the Ediacaran, Edward Albert Group to the south (Corkeron, 2007; Plumb *et al.*, 1981). The early Cambrian (505 ± 2 Ma) Antrim Plateau Basalt overlies Kinevans Sandstone and Ranford Formation (Dow & Gemuts, 1969; Evins *et al.*, 2009; Jourdan *et al.*, 2014; Marshall *et al.*, 2016), and is in turn overlain by Cambrian marine rocks dated by trilobites (Kruse *et al.*, 2004; Öpik, 1970), and poorly fossiliferous sandstones of presumed Devonian age (Mory & Beere, 1985).

Materials and methods

Zebra rock was obtained from four localities around Lake Argyle: (1) Duncan Road at S16.12519° E129.04961°, (2) Donkey Creek at S16.0622° E128.96213°, (3) Remote Island at S16.304335° E128.755815°, and (4) Snappy Gum Ridge at S16.359677° E128.718314° (Figure 1). Strata at Duncan Road and Donkey Creek are flat lying (Figure 4c), but dip is near vertical at Remote Island and Snappy Gum Ridge (Figure 3b). Another locality (#3 in Figure 1) near Mt Misere near Argyle Downs Station recorded by Loughnan and Roberts (1990) is now submerged under Lake Argyle. Whole beds of zebra rock were cut and polished, and thin-sections prepared (Figure 3). Measured sections and rock collections were made in quarries at Duncan Road and Donkey Creek (Figure 4), as well as in Moonlight Valley near Warnum (Figures 5 and 6).

Oriented rock samples were collected for laboratory studies of bulk chemical composition (Supplementary Information Table S1), trace element composition (Table S2), and thin-section petrography (Figure 7). Thin-sections were used to quantify grainsize (Table S3) and mineral compositions (Table S4) by point counting (500 points) using a Swift automated point counter on a Leitz Orthoplan Pol research microscope. Accuracy of such point counts is ± 2% for common constituents (Murphy, 1983). Major element chemical analysis was used to characterise chemical weathering trends and metamorphic alteration (Figures 8 and 9), determined by X-ray fluorescence at ALS Chemex in Vancouver, Canada, and rare earth elements by inductively coupled plasma atomic emission spectrometry (ICP-AES) in the same laboratory. Ferrous iron was determined by potassium dichromate titration, and total iron as ferric adjusted for that molar proportion. Bulk density was measured by the clod method: from raw weight, then weight in and out of chilled water of paraffin-coated clods.

Metamorphic and diagenetic alteration

Three common early burial alterations were found in the Ranford Formation and upper Moonlight Valley Tillite, comprising (1) drab-spotting of upper portions of beds owing to burial gleisation of organic matter, (2) dark red (Munsell 10 R) colour from dehydration reddening of ferric hydroxide minerals (Figure 3), and (3) substantial lithostatic compaction (Retallack, 1991a). Burial gleisation is chemical reduction of oxides and hydroxides of iron by anaerobic bacteria on subsidence into anoxic water, and is especially suggested by drab mottles and tubular features radiating down from bed tops (Figure 5b, d), as in Cambrian (Álvaro *et al.*, 2003; Retallack, 2008) and Proterozoic red beds (Driese *et al.*, 1995; Retallack, 2013). Such geologically ancient red beds are also purple to red in colour from burial dehydration of ferric oxyhydroxides (Figure 3), unlike brown to yellow modern soils and late Pleistocene sediments (Retallack, 1991a).

The uppermost Moonlight Valley Tillite 'cap carbonate' and lower Ranford Formation sandstones have abundant dolomite, both microcrystalline and as silt-sized irregular grains and rhombs. The rhombs are limpid, and not like dolomite replacing other grains, nor forming an interlocking cement, nor baroque with curved cleavage (Mehmood *et al.*, 2018). The microscopic appearance of this 'cap carbonate' is comparable with the Nuccaleena Formation, the basal Ediacaran 'cap carbonate' of South Australia, where micrite and other silt size grains appear to have been loess, with limited burial neomorphism (Retallack, 2011). Correlation of $\delta^{13}C$ and $\delta^{18}O$ in these dolomites is also highly significant as in soils, unlike weak relationships seen in marine or lacustrine limestones altered by meteoric diagenesis (Figure 10).

One index of lithostatic compaction is the Weaver index of 10 Å/10.5 Å peak height on XRD traces of 3.3 ± 0.2 for the specimens of zebra rock studied by Loughnan and Roberts (1990). This degree of recrystallisation has not resulted in excessive potash metasomatism (Novoselov & de Souza Filho, 2015), because potash enrichment is not seen in tau analysis (Figure 8). A Weaver Index of 3.3 for Ediacaran rocks of the Flinders Ranges of South Australia corresponds to burial depth of 3.6 ± 0.4 km (Retallack, 2013). This is less than 4.4 km of observed overburden in Western Australia (Figure 2), because the Albert Edward Group was not deposited this far north (Mory & Beere, 1985; Plumb *et al.*, 1981). Weaver indices of zebra rock are within the anchizone of diagenesis, but not metamorphic (Frey, 1987), as also suspected from shallow dips, except for the Remote Island and Snappy Gum Ridge localities (Figure 3b). Lack of metamorphism is also indicated by low thermal stability of remnant magnetisation of zebra rock (Abrajevitch *et al.*, 2018). Burial compaction (*C* as a percentage) expected for 3.6 km burial can be calculated as 58%. These calculations use the following formula with depth of burial (*B* in km) and 0.51, 0.49 and 0.27 as physical constants (of Sheldon & Retallack, 2001) also used to calculate compaction of comparable Ediacaran red beds of the Flinders Ranges, South Australia (Retallack, 2013).

$$C = \frac{-0.51 \times 100}{\left\{\left(\frac{0.49}{e^{\frac{B}{0.27}}}\right) - 1\right\}} \quad (1)$$

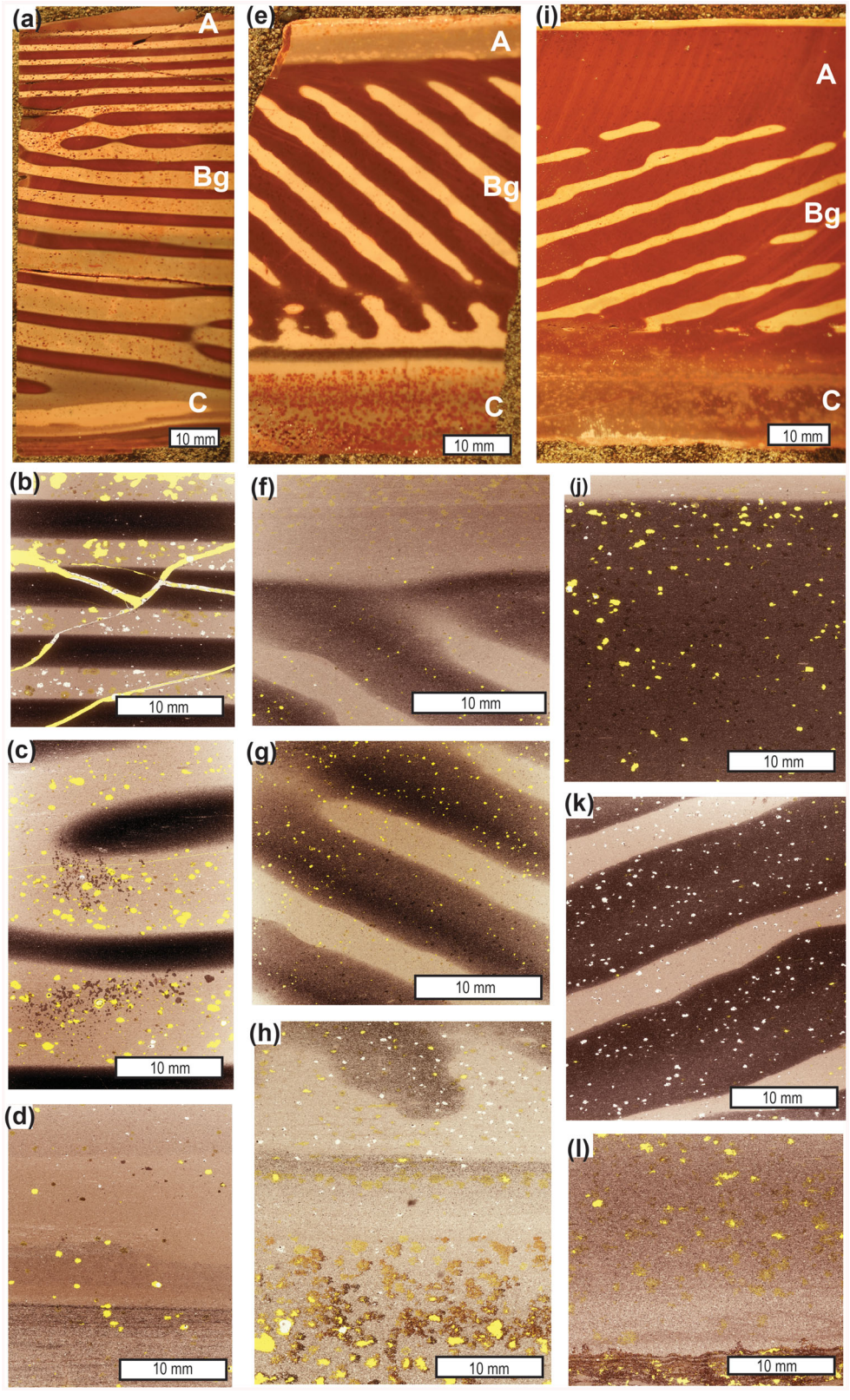

Figure 3. Zebra rock profiles in polished sections and thin-sections from Duncan Road (a–d), Remote Island (e–h) and Lake Argyle (i–l). Yellow epoxy reveals cracks and missing grains.

Figure 4. Field photographs of zebra rock localities in Johnny Cake Member of Ranford Formation: (a) Ruth Duncan with zebra rock from the Duncan Road Quarry; (b) three zebra rock beds tilted vertical at the Snappy Gum Ridge locality; (c) cross-sections (at arrows) of gypsum pseudomorphs in the Thamberalg paleosol at Donkey Creek; (d) gypsum desert roses from Donkey Creek; and (e) aquatic microbially induced sedimentary structure (MISS) *Rugalichnus matthewi* from Donkey Creek. Scales at base of (d, e) are graduated in millimetres. Photo (b) courtesy of Brian Fennell.

Sedimentary facies

TC: trough cross-bedded dolomitic sandstone

Thick (1–2 m) beds of trough cross-bedded, medium to coarse sandstone in the lower Ranford Formation and upper Moonlight Valley Tillite at Moonlight Valley are prominent cliff-forming units (Figure 5a). From a distance, they can be seen to be lenticular in geometry, with flat tops, but bottoms variably eroding down into underlying beds (Figure 5a). Their bases include angular clasts of redeposited dolomite-cemented sandstone and red claystone breccia, which are intraformational clasts identical to other interbedded layers, including the red clayey Moonlight Valley Tillite.

Trough cross-bedding is created within sand bars confined by channels of rivers (Cant & Walker, 1978) and deltaic distributaries (Gastaldo *et al.*, 2009). A river interpretation is compatible with the diversity of intraformational clasts suggestive of erosional banks rather than constructional deltaic distributaries.

RG: red-green siltstone

This is a facies of purple-red siltstone finely interbedded with grey-green siltstone beds. Individual beds are mostly 1–4 mm thick. Some units 15–20 cm thick are more massive with grey-green mottles on the top, but most of the bed is red (Figure 5b, c), and others contain gypsum rosettes (Figure 4c, d). Horizontal planar and wavy bedding are the main sedimentary structures, but there are also straight-crested ripples, shallow hexagonal mud cracks and thin

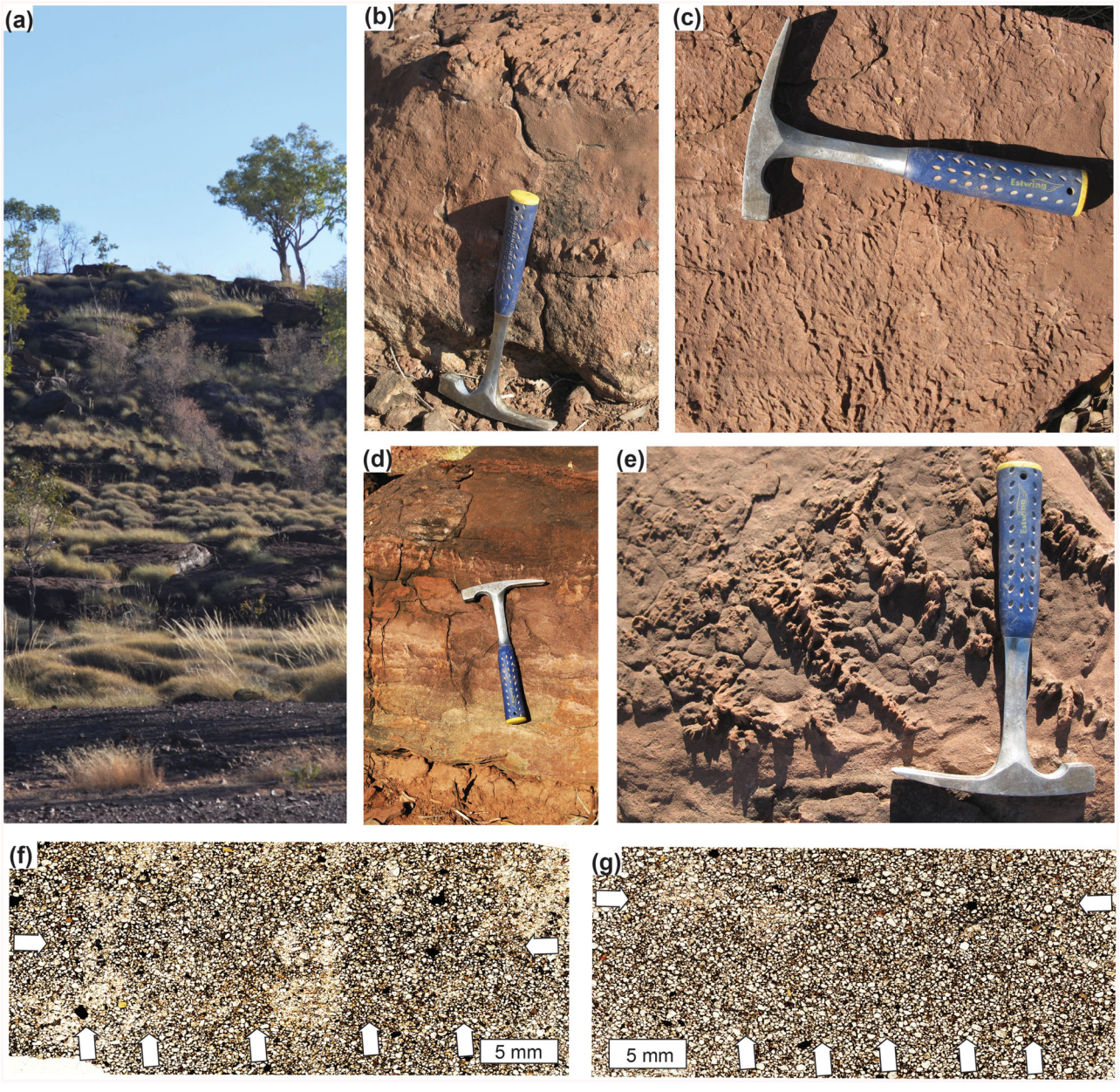

Figure 5. Field photographs (a–e) and thin-sections (f, g) of cap carbonate of the Moonlight Tillite east of Warnum: (a) measured section locality with Moonlight Tillite in flats of foreground, cap carbonate in lowest bench and Jarrad Member of Ranford Formation on skyline; (b, c) Jilam paleosol in cross-section (b) and surface texture of *Rivularites repertus* (c); (d, e) Galadil paleosol in cross in section (d) and surface with *Yangtziramulus zhangi* (e). Thin-sections R5753 (f) and R5754 (g) show vertical cross-sections of *Yangtziramulus zhangi* with interior chambers filled with dolomite rhombs and dark organic partitions.

claystone breccias. Mud cracks from RG facies have been illustrated by Lan and Chen (2013).

The fine interlayering of red oxidised and green reduced layers, and claystone breccias with both green and red clasts are evidence that both oxidation and reduction occurred during the Ediacaran (Mawson & Segnit, 1949), rather than oxidation only in outcrop (Gehling, 2000). Lacustrine environments for RG facies are suggested by persistent planar bedding and undulose microbially induced sedimentary structures attributed to aquatic microbial mats (*Rugalichnus matthewi* of Stimson *et al.*, 2017). These lakes would have been shallow and well aerated to permit alternating oxidation and reduction, and episodic desiccation to produce mud cracks.

IR: interbedded red siltstone and sandstone

Capping beds to facies TC of trough-bedded sandstone commonly includes medium to coarse sandy flagstone beds 5–10 cm thick, with interbedded fine-grained sandstones and siltstone, known as interflag sandstone laminae (Figures 5b, c and 6a). Planar bedding, wavy bedding and ripple marks are common, as well as claystone breccias. IR

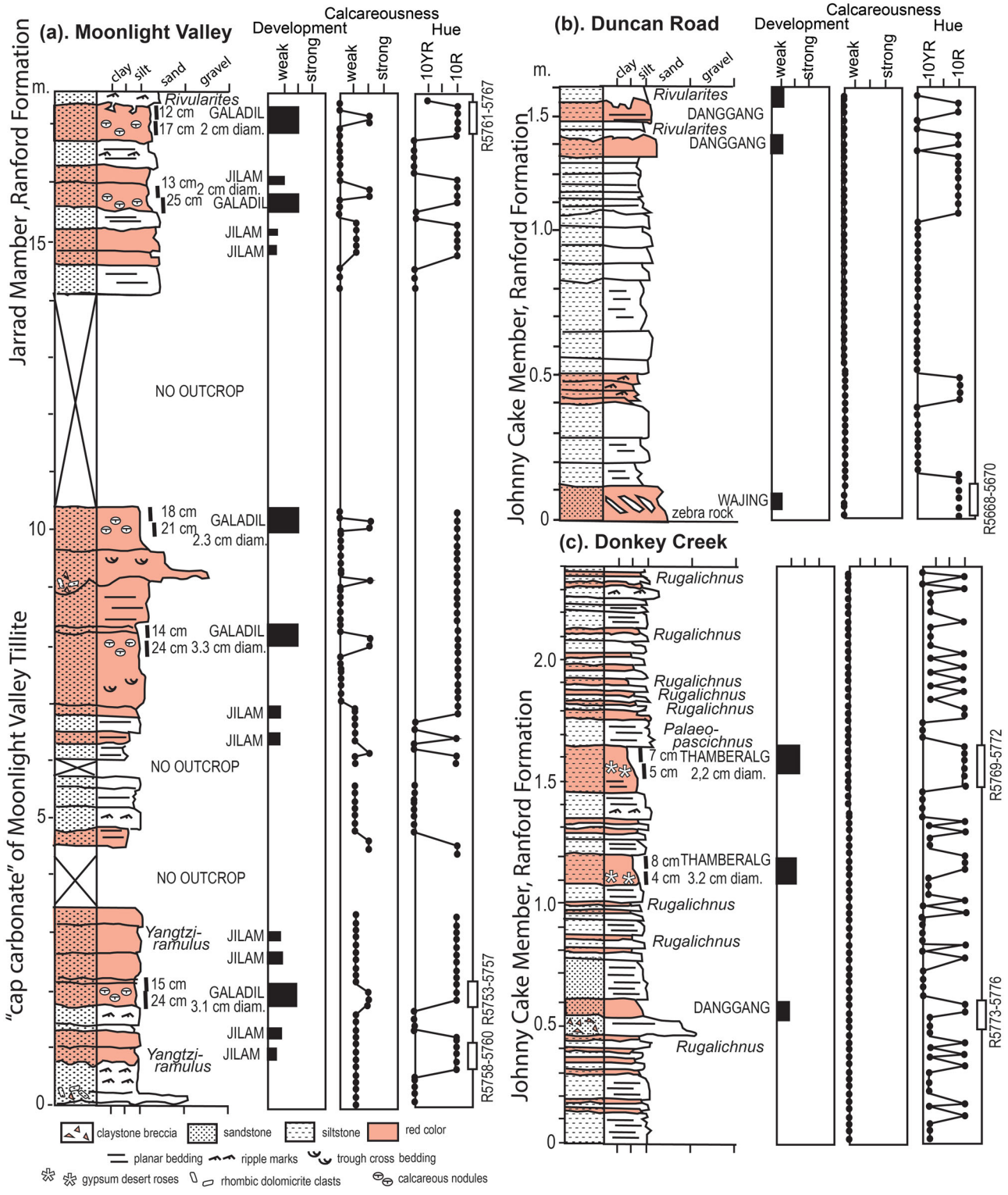

Figure 6. Measured sections east of Warnum (a) and in quarries of Donkey Creek (b) and Duncan Road (c).

facies also has strongly textured surfaces informally known as 'old elephant skin', and as the microbial trace fossil *Rivularites repertus* (Retallack & Broz, 2020).

The IR facies with interflag sandstone laminae (Retallack, 2019) and *Rivularites repertus* (Retallack & Broz, 2020) is interpreted as fluvial levee, in part from its close association with paleochannel facies TC. The fine-grained laminae are considered eolian reworking of levees during the interval between floods (Retallack, 2019). *Rivularites repertus* is a texture of microbial earths (Retallack, 2012a) with evidence of multiple episodes of cracking and healing, owing to desiccation alternating with rehydration by rain

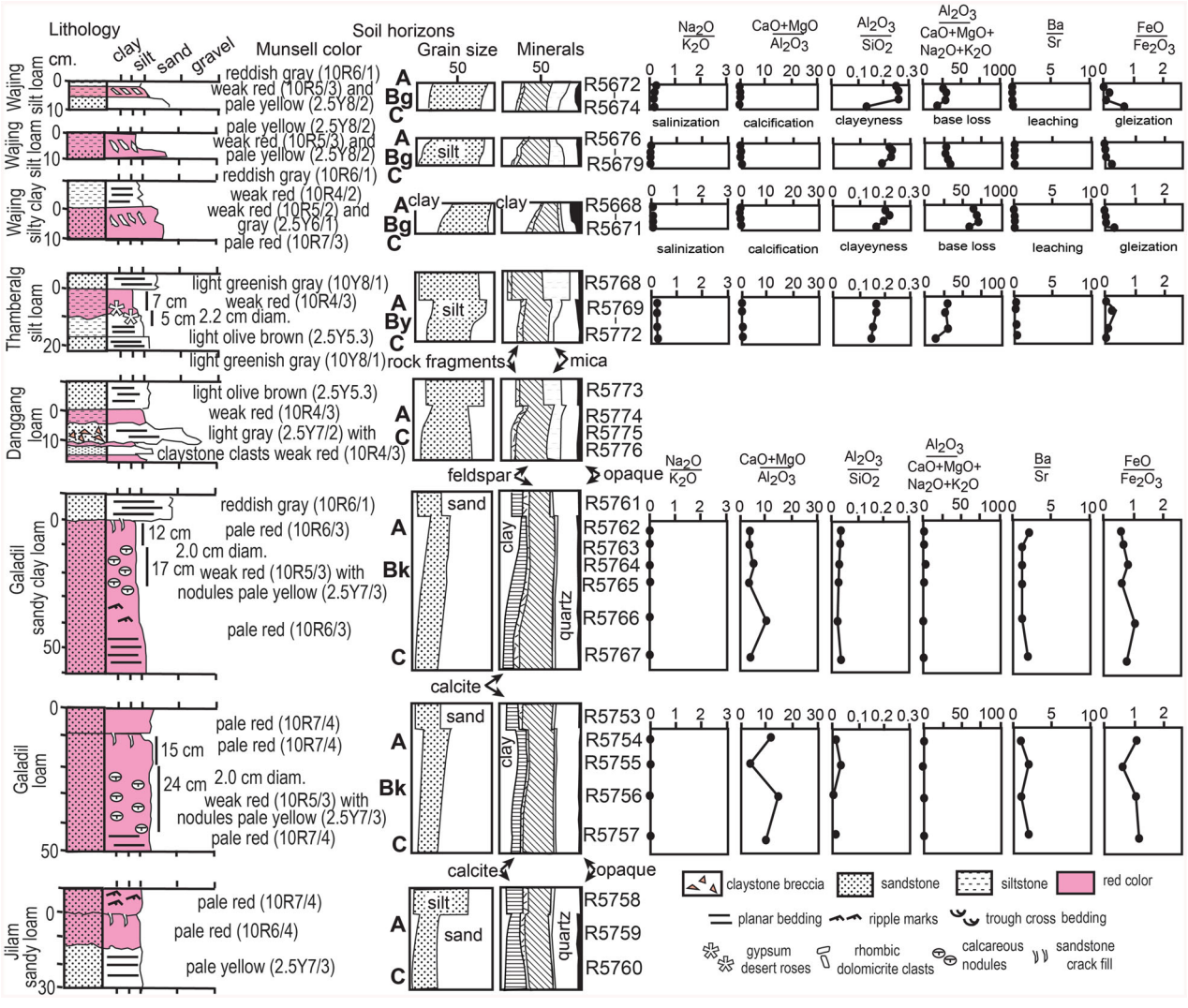

Figure 7. Paleosol profiles, and their petrographic and chemical composition.

and flooding (Figure 11c, d). Aquatic microbial mats by contrast are undulose to stromatolitic (Stimson *et al.*, 2017)

RS: red sandstone with dolomitic nodules

Dolomitic nodules of the red sandstone facies are found both in place within thick sandstone beds and redeposited into conglomeratic stringers of paleochannels of facies TC. Thus, they were cemented with dolomite during the Ediacaran and not subsequently.

The micritic cement and rounded form of these nodules within a red matrix (Figure 5d) are similar to soil carbonate, also known as caliche (Retallack, 2015a, 2015b). Furthermore, the nodules are arranged not at the erosional surface of the bed, but a set distance below the top of the bed, as is typical for soil calcic (Bk) horizons (Retallack, 2005) of modern soils (Figure 11f). Carbonate nodules in marine rocks are distinct in generally larger size, enclosing marine fossils, grey to green matrix, and lack evidence of redeposition because they formed during burial (Gariboldi *et al.*, 2015). These nodular profiles thus represent well drained floodplain environments.

Paleosol recognition

Paleosols are definitively recognised in the field by fossil root traces (Retallack, 1976, 1991b), but vascular land plants did not exist before the Silurian (Retallack, 2015a). Lack of root traces may be why not a single Ediacaran paleosol was recognised until 2011, although hundreds of Ediacaran paleosols have been described since then (Retallack, 2016). Field recognition of Precambrian paleosols relies on soil structures (Figures 3–5) and soil horizons (Figures 6 and 7). Special features of Precambrian paleosols may also include surface textures characteristic of microbial earth soils (*Rivularites repertus* of Retallack & Broz, 2020) and eolian interbeds (interflag sandstone laminae of Retallack, 2019). The following paragraphs consider each of these criteria in turn.

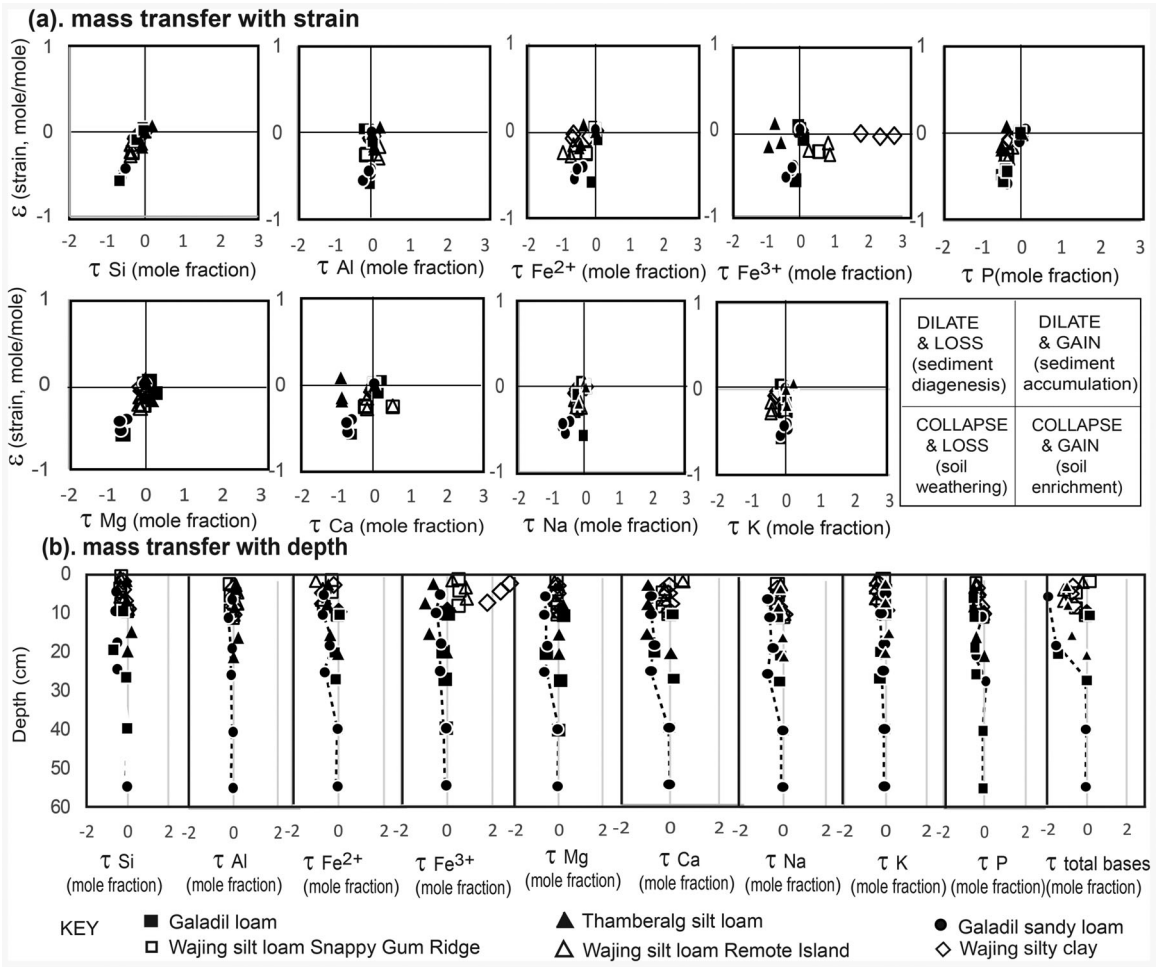

Figure 8. Tau analysis of elemental mass transfer *vs* strain (a) and *vs* depth in paleosol profiles (b).

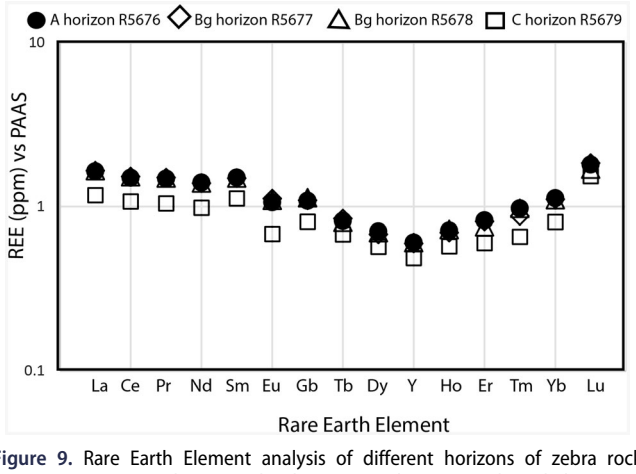

Figure 9. Rare Earth Element analysis of different horizons of zebra rock from Snappy Gum Ridge normalised to post-Archean Australian Shale (Nance & Taylor, 1976).

Crack patterns

Desiccation cracks have a V-shaped profile in clay (Weinberger, 2001), and several examples in shales of facies IR of the Johnny Cake Member of the Ranford Formation have been illustrated by Lan and Chen (2013). Similar tapering cracks were also seen in the dolomitic sandstones of the upper Moonlight Valley Tillite and Jarrad Member of the Ranford Formation (Figure 5b, d). These sandstone cracks emanate from the most hematite-rich tops of sandy beds but are filled with fine-grained white dolomitic sandstone. How sand can crack like clay is explained by Prave (2002) as owing to abundant hydrated microbiota, like that of a thick microbial earth soil rather than thin microbial mat (Retallack, 2012a). This idea is supported by co-occurring microbially influenced sedimentary structures (MISS of Noffke, 2010), such as the microbial trace fossil *Rivularites repertus* (Retallack & Broz, 2020), which has complex, multiple fills of shallow cracks (Figure 5c). A comparable phenomenon is oscillating desiccation cracks of modern supratidal flats (Noffke, 2010), which is the depositional setting envisaged by Lan and Chen (2013).

Sand crystals

Rosettes of gypsum with included detrital grains in the Johnny Cake Member of the Ranford Formation (Figure 4d) have attracted attention as possible Ediacaran discoid fossils (Dunnet, 1965), which have been variously interpreted

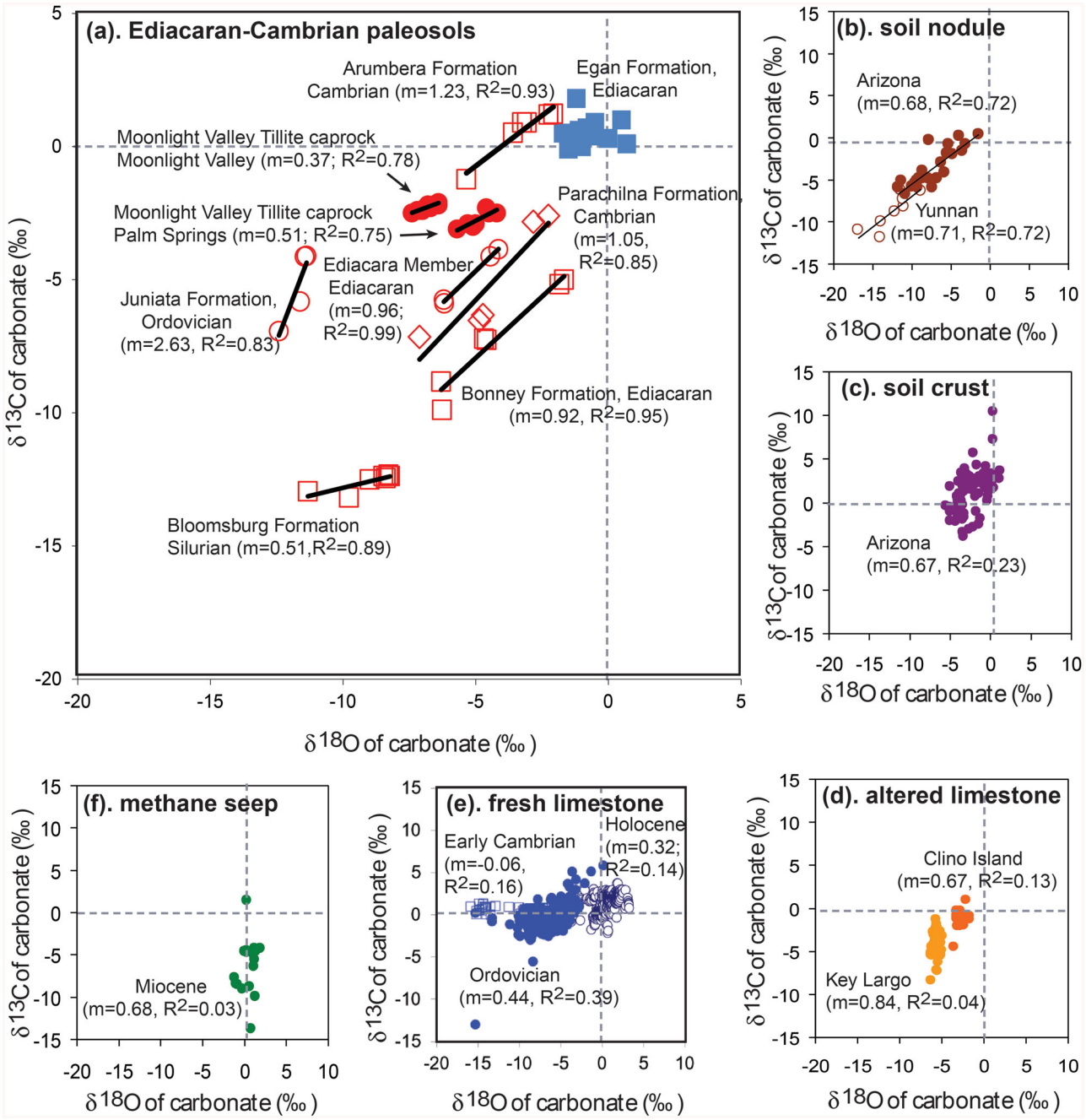

Figure 10. Covariation of carbon and oxygen isotopic composition of carbonate as a characteristic of paleosols, rather than other settings: (a) early Ediacaaran cap carbonate of Moonlight Valley Tillite at two localities (Bao *et al.*, 2012), Ediacaran and Cambrian paleosols of South Australia (Retallack *et al.*, 2014), Cambrian Arumbera Formation at Ross River (Retallack & Broz, 2020). Ordovician paleosols of Pennsylvania (Retallack, 2015a), and Silurian paleosols of Pennsylvania (Retallack, 2015b); (b) soil nodules (above Woodhouse lava flow, near Flagstaff, Arizona) (Knauth *et al.*, 2003) and in Yuanmou Basin, Yunnan, China (Huang *et al.*, 2005); (c) soil crusts on basalt (Sentinel Volcanic Field, Arizona, from Knauth *et al.*, 2003); (d) Quaternary marine limestone altered diagenetically by meteoric water (Key Largo, Florida, Lohmann, 1988; Clino Island, Bahamas, Melim *et al.*, 2004); (e) Holocene (open circles) and Ordovician (open squares) unweathered marine limestones (Veizer *et al.*, 1999) and lower Cambrian (closed circles), Ajax Limestone, South Australia (Surge *et al.*, 1997); (f) marine methane cold seep carbonate (Miocene, Santa Cruz Formation, Santa Cruz, California (Aiello *et al.*, 2001). Slope of linear regression (*m*) and coefficients of determination (R^2) show that carbon and oxygen isotopic composition is significantly correlated in soils and paleosols.

as fossil jellyfish (Sprigg, 1949) or microbial colonies (Grazhdankin *et al.*, 2012). The Ranford rosettes have been debunked as fossils by Grey (1981a, 1981b) and Lan and Chen (2012), primarily because of their radiating crystal structure like desert roses (Almohandis, 2002; Jafarzadeh & Burnham, 1992), although some have a degraded concentric appearance like Ediacaran discoids (Sprigg, 1949). Their occurrence well below the truncated upper surface of beds (Figure 4c) is comparable with gypsic horizons (Figure 11e) of desert soils (Retallack & Huang, 2010). Sand crystals form only in soils, and not in marine or lacustrine evaporites, nor in intertidal sabkhas, where saturated sediment allows clear crystals to grow by displacement of grains (Renaut & Tiecerlin, 1994; Ziegenbalg *et al.*, 2010).

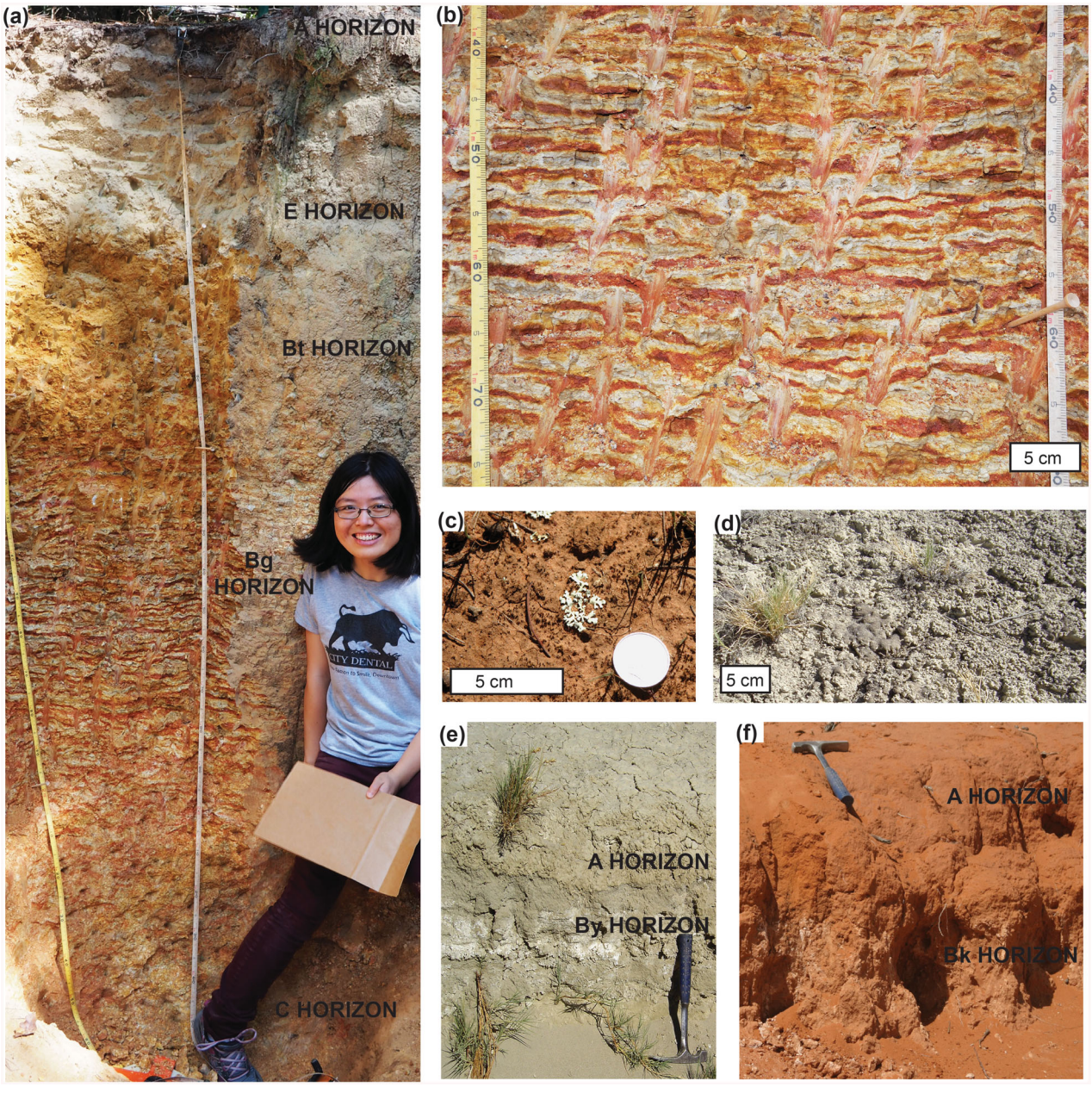

Figure 11. Modern soil analogues for Ediacaran paleosols: (a, b) redox banding in Udult (Cataula sandy loam soil) near Union, South Carolina (N34.60806° W81.72205°; Chen *et al*., 2019); (c) microbial earth with light green foliose lichen (*Xanthoparmelia reptans*), and faecal pellets on red soil between red mallee (*Eucalyptus socialis*) and porcupine grass (*Triodia scariosa*) near Damara station, New South Wales (Retallack, 2012b; S34.154198° E143.329838°); (d) microbial earth with greasewood (*Sarcobatus vermiculatus*), Black Rock Desert, Nevada (Retallack, 2012a; N40.97351° W119.00808°); (e) Gypsid (Bubus fine sandy loam) soil Black Rock Desert, Nevada (N40.80440° W119.18861°); (f) Calcid soil near Damara Station, New South Wales (as for c). Images a and b courtesy of C. W. Cook, with permission.

Interflag sandstone laminae

Thin laminae of fine-grained sandstone and siltstone cap thick cracked beds of dolomitic sandstone in the Moonlight Valley Tillite and Jarrad Member of the Ranford Formation (Figures 5b and 6a), and appear to be interflag sandstone laminae (Retallack, 2019). In the Johnny Cake Member of the Ranford Formation some thin siltstone layers show inverse grading (Figure 3d), characteristic of climbing translatent bedding formed by wind (Hunter, 1977). Traction currents of modern river flooding produces medium-grained beds, and these alternate with fine-grained laminae from wind reworking during the interval of a year or more between floods (Draut & Rubin, 2008; Draut *et al*., 2008). Wind redeposition is evidence of sub-aerial exposure, which is also a requirement for paleosols.

Zebra rock

Zebra rock is a clayey siltstone bed, 5–15 cm thick, with alternating diffuse red and grey bands, 4 to 25 mm thick, varying from subhorizontal to angles up to 50° from regional bedding (Figures 3 and 4a, b). These distinctively

banded rocks can form successive beds (Figure 4b), or occur singly (Figure 4a), within the Johnny Cake Member of the Ranford Formation. The Duncan Road quarry exposes zebra rock 90 m along strike and it varies in thickness considerably, pinching out in places and elsewhere swelling to thickness of 15 cm. Less marked lateral variation in thickness is also seen in the Snappy Gum Ridge quarry (Figure 4b). Tops of the zebra rock bed are red and overlain abruptly by coarse-grained grey sandstone (Figure 3a, e, i). The bottoms of the zebra rock bed are grey sandstone (Figure 3d, h, l), although that grey colour can be obscured by pits remaining from pyrite ferruginised in the modern outcrop (Figure 3e). Gleisation as indicated by ferrous/ferric ratios >1 is found at the base, not at the top of the bed (Figure 7). Two of the zebra rocks analysed had very high proportion of mica, but this was less abundant in a third example, and all three showed strong depletion of feldspar toward the top of the bed (Figure 7). Both molecular weathering ratios (Figure 7) and tau analysis (Figure 8) of major elements show that zebra rock is intensely weathered from the surface down, as also indicated by identification of the main components as quartz, kaolinite and dickite, with minor sericite and alunite (Loughnan & Roberts, 1990). Ferrihydrite has been detected in zebra rock by electron paramagnetic resonance in both red and white regions (Boas *et al.*, 2005). Intense leaching also is supported by REE enrichment toward the top, without fractionation of light *vs* heavy REE (Figure 9). Red bands have 30 wt% iron as Fe_2O_3, but drab bands have less than 1 wt% iron largely as FeO (Table S1). Loughnan and Roberts (1990) found a disparity of 8–9 wt% total iron in red bands, but only 0.5 and 0.07 wt% in the white bands. Some remnant paleomagnetic directions in zebra rock and associated sediments can be identified as Paleozoic overprints, but zebra rock has a very distinctive paleomagnetic orientation regarded as primary Ediacaran by Abrajevitch *et al.* (2018).

Several past hypotheses for the origin of zebra rock can now be dismissed. Low metamorphic grade and primary paleomagnetic signal (Abrajevitch *et al.*, 2018; Loughnan & Roberts, 1990) is evidence against formation by hydrothermal mineralising solutions (Kelka *et al.*, 2017). Multiple horizons of zebra rock tipped on end (Figure 4b) are evidence against liesegang banding induced by weathering of bedrock (Hobson, 1930), or within a single unconformity paleosol (Trainer, 1931). Liesegang bands are asymmetric with intensity increasing gradually then ceasing abruptly and follow the outlines of joint blocks or clasts (Sadek *et al.*, 2010), unlike zebra rock (Figure 3); nor do the bands correspond to variations in grainsize (Figure 3) to support a primary depositional origin as cross-bedding (Geidans, 1981; Larcombe, 1925, 1927).

In contrast, zebra rock beds are thicker and more massive than associated shaley laminae (Figures 4b and 6b) as if each bed were deposited in one episode as an airfall crystal tuff, and in two cases as a biotite tuff (Figure 7). Once in place, profound chemical weathering (Figure 7) and paleomagnetic characters (Abrajevitch *et al.*, 2018) are evidence that they were soils comparable with modern gleyed soils near Union, South Carolina (Figure 11a, b). This distinctive grey-red banding in soils within diffuse margins comparable with zebra rock (Figure 3) is considered the result of gleisation of a red soil by pockets of anaerobic bacteria active during waterlogging (Chen *et al.*, 2019), like other examples of soil gleisation (Schulz *et al.*, 2016). It is the opposite of conservation of total iron in red and grey areas of paleosols with closed-system burial gleisation (Retallack, 1991a). Loss of iron in white bands of zebra rock by open system reduction down to reduced lower horizons is compatible with groundwater rather than surface-water gleisation (Vepraskas & Sprecher, 1997). Soil lamellae are another comparable feature, but these ferruginised seams within soils are much more sandy than zebra rock (Bockheim & Hartemink, 2013; Rawling, 2000). An alternative view of Mattievich *et al.* (2003) is that zebra rock formed as a liquid crystal in which hematite grains in the tens of nanometre size range had sufficient magnetic moment to segregate within a colloidal bed under a normal intensity of Earth's magnetic field. Evidence against this is the preservation of sand and silt grains in zebra rock (Figure 3), which were far from colloidal, with no more than 50% grains of clay or finer grainsize (Figure 7; Table S3). Among these grains are oxidised pyrite, supporting the idea of acid sulfate soil weathering to account for the localised intensity of weathering of thin zebra rock beds (Loughnan & Roberts, 1990).

Mineral weathering trends

Point counting of individual beds shows surface depletion of rock fragments and feldspar in proportion to degree of destruction of bedding, especially marked within the thin zebra rock beds (Figure 7). Clay enrichment is commonly abrupt below sharp grainsize discontinuities with overlying sandstone and confined to intervals only 5–15 cm thick, unlike alteration by symmetrical hydrothermal or diffuse metamorphic alteration (Kelka *et al.*, 2017; Wallace & Hood, 2018). This is best explained as the result of hydrolytic weathering to clay of feldspar within soil profiles (Retallack, 2013, 2019). These abrupt contacts are well-developed soils overlain sharply by fluvial sandstones.

These trends are also seen in sandstones of the upper Moonlight Valley Tillite and Jarrad Member of the Ranford Formation, which contain large amounts of silt size dolomite (Figure 7). Dolomite is depleted near the top of the profiles but is very abundant at the base of beds as well. Some leaching of dolomite during soil formation is likely, but such substantial amounts of dolomite are evidence that this mineral was also detrital, either eolian or fluvial.

Chemical weathering trends

Molar weathering ratios do not show the erratic depth functions of chemically distinct sedimentary beds, but relatively smooth trends compatible with soil formation of two divergent kinds (Figure 7). Uniformly low soda/potash ratios are evidence against salinisation in these beds. Alkaline earths/alumina spike in dolomitic nodules of two Galadil profiles so are evidence for calcification, but the zebra rocks (Wajing and Thamberalg) are non-calcareous. Hydrolysis of feldspar to clay is revealed by increases in alumina/silica and alumina/bases at the tops of profiles, especially marked in the zebra rocks (Wajing and Thamberalg profiles), but not in the dolomitic profiles (Galadil). Ba/Sr molar ratios as evidence of chemical leaching are low in dolomitic profiles (Galadil), but very low in the zebra rocks (Wajing and Thamberalg). Low ferrous/ferric iron confirms red colour from hematite is evidence of oxidising conditions, especially in zebra rocks (Wajing and Thamberalg), but the dolomitic (Galadil) profiles show modest chemical reduction (gleisation; Retallack, 1991a). Oxidation during the Ediacaran, rather than in modern outcrop, is indicated by red claystone clasts redeposited within grey sandstones (Figure 8).

Rare earth elements show modest enrichment toward the surface with only slight rare earth enrichment in a Wajing profile (Figure 9), as in many other Precambrian arid land paleosols (Retallack, 2018; Retallack & Mao, 2019). Comparable enrichment slightly favouring light rare earth elements is also seen in modern aridland loessial soils (Compton *et al.*, 2003; Ramakrishnan & Tiwari, 1999), unlike depletion seen in humid granitic soils (de Sá Paye *et al.*, 2016; Kurtz *et al.*, 2001). There is a slight negative europium anomaly, as in sediments from granitic (Foden *et al.*, 1984), rather than basaltic rocks (Bavinton & Taylor, 1980). There is no marked enrichment in europium as in hydrothermally altered rocks (Bolhar *et al.*, 2005; Sugahara *et al.*, 2010). Nor are rare earth elements unchanged within the bed as in marine deposition and halmyrolytic alteration of marine beds (Clauer *et al.*, 1990; Setti *et al.*, 2004).

Tau analysis

A definitive method to disentangle soil formation from sedimentation is tau analysis (Brimhall *et al.*, 1992). Tau analysis deconstructs two separate aspects of weathering: mole fraction mass transport ($\tau_{j,w}$) of a mobile element and mole fraction strain ($\varepsilon_{i,w}$) of an immobile element (Ti used here), using the following formula including bulk density (ρ in g.cm^{-3}) and oxide assay (C in weight %) for successive samples (subscripts *i*, *j*) of weathered material (subscript *w*) and parent material (subscript p).

$$\varepsilon_{i,w} = \left[\frac{\rho_p C_{j,p}}{\rho_w C_{j,w}}\right] - 1 \quad (2)$$

$$\tau_{j,w} = \left[\frac{\rho_w C_{j.w}}{\rho_p C_{j,p}}\right][\varepsilon_{i,w} + 1] - 1 \quad (3)$$

Soils and paleosols lose mass with weathering and so have negative strain ($\varepsilon_{i,w} < 0$), and also lose nutrient cations and silica, so have negative mass transfer ($\tau_{j,w} < 0$). In contrast, sediment accumulation and diagenetic alteration other than weathering adds elements and mass so has positive strain and mass transfer. Tau analysis has been widely used for Precambrian paleosols (Liivamägi *et al.*, 2014; Retallack & Mindszenty, 1994), as well as Cenozoic paleosols (Bestland *et al.*, 1996; Sheldon, 2003), and modern soils (Chadwick *et al.*, 1990; Hayes *et al.*, 2019). On this basis, most analyses of beds within the Moonlight Valley Tillite and Ranford Formation are within the collapse and loss quadrant, with the exception of iron enrichment of red, but not drab parts of zebra rocks (Wajing of Figure 8a). Zebra rock beds are thin but show profound chemical differentiation. In contrast, deep depletion from the surface is well demonstrated by dolomitic profiles (Galadil of Figure 8b).

Stable isotopic correlation

Analyses of dolomitic nodules in the Ediacaran 'cap carbonate' of the upper Moonlight Valley Tillite at both Moondlight Valley and Palm Springs by Bao *et al.* (2012) show significant correlation of $\delta^{13}C$ and $\delta^{18}O$ values like other Ediacaran and Paleozoic paleosols (Figure 10a), and Holocene soils (Figure 10b) in China (Huang *et al.*, 2005) and Arizona (Knauth *et al.*, 2003). Less statistically significant correlations (Figure 10c, d) are found in soil carbonate crusts (Knauth *et al.*, 2003), and marine limestone altered by deep circulation of meteoric water (Lohmann, 1988; Melim *et al.*, 2004). Although similar relationships in seasonally dry lake carbonates have been attributed to mixing of distinct fluid sources (Talbot, 1990), these may also be cases of alteration by meteoric weathering during lake low stands. In contrast, unaltered marine limestones and sea shells (Figure 10e) and perennial lake carbonates show no hint of correlation (Surge *et al.*, 1997; Talbot, 1990; Veizer *et al.*, 1999), and near constant $\delta^{18}O$ values but highly varied $\delta^{13}C$ values (Figure 10f) is created by microbial methanogenesis in carbonate of marine methane seeps (Aiello *et al.*, 2001; Peckmann *et al.*, 2002), and siderite of wetland paleosols (Ludvigson *et al.*, 1998, 2013). The position of data within this cross-plot is determined by a variety of paleoenvironmental factors, especially temperature and CO_2 partial pressures, but it is the tightness of the correlation that distinguishes paleosols.

Such tight correlations of $\delta^{13}C$ and $\delta^{18}O$ values are not accidental, but owing to selection for light isotopologues of CO_2 (Retallack, 2016). This may be due to kinetic evaporative effects in narrow spaces of soils (Ufnar *et al.*, 2008), but is more likely related to stomatal conductance and fractionation during photosynthesis by the enzymes

rubisco and carbonic anhydrase because $\delta^{13}C$ and $\delta^{18}O$ covariance is seen in respired soil CO_2 (Ehleringer & Cook, 1998; Ehleringer *et al.*, 2000), and in plant cellulose (Barbour & Farquhar, 2000; Barbour *et al.*, 2002). A role for stomates is undermined by strong correlation of $\delta^{13}C$ and $\delta^{18}O$ values in early Paleozoic and Ediacaran paleosols, because they predate the evolution of stomates (Figure 10). Similar covariance of $\delta^{13}C$ and $\delta^{18}O$ values is found in Ediacaran carbonate in the Fauquier Formation of Virginia (Hebert *et al.*, 2010), and the Shibantan Member of the Dengying Formation of China (Duda *et al.*, 2014). The covariance is not destroyed by metamorphism to greenschist facies in paleosols of the Juniata and Bloomsburg formations (Retallack, 2015a, 2015b).

Values of $\Delta^{17}O$ found in carbonate associated sulfate of the Moonlight Valley Tillite by Bao *et al.* (2012) are so low that they would not have been preserved in either marine or freshwater. Such mass independent fractionations are only preserved in terrestrial tuffs (Bindeman *et al.*, 2007; Martin & Bindeman, 2009). This is evidence that the Moonlight Valley Tillite 'cap carbonate' in its type section was a terrestrial deposit.

Paleosol interpretation

The preceding paragraphs are evidence for a variety of paleosols in the Upper Moonlight Valley Tillite and Ranford Formation. The remainder of this paper develops paleoenvironmental conclusions based on these paleosols. The various kinds of beds analysed as putative paleosols have been named (Table 1) using the Miriwoong (for Lake Argyle) and Gija (for Warnum) aboriginal languages (Jarraggirrem, 2017; Olawsky & Kofod, 2019). Despite burial illitisation, these pedotypes can now be interpreted in terms of soil taxonomy and various soil-forming factors to build a detailed model of their paleoenvironment (Table 2; Figure 12).

Paleosol identification

Thamberalg profiles with cracked surface (A horizon) over a diffuse horizon with mottles and sand crystals (By or gypsic) are most like Gypsids (Soil Survey Staff, 2014). Galadil profiles, on the other hand, have cracked surfaces (A horizon) over a deep horizon (Bk or calcic) of pedogenic carbonate nodules, as in Calcids (Soil Survey Staff, 2014). Comparable considerations can be used to classify these paleosols in other classifications (Table 1) of Australia (Isbell, 1996; Stace *et al.*, 1968), and of the Food and Agriculture Organization (1978). Other profiles are less well developed Entisols and Inceptisols (of Soil Survey Staff, 2014), and would have been restricted to disturbed parts of the landscape (Table 2).

In the Food and Agriculture Organisation map classification (Food and Agriculture Organization, 1978) the best-developed soil type of the Jarrad Member of the Ranford Formation was Orthic Solonchak, this soil assemblage would have a map code of Zo + Jd,Gd (Table 1). The closest modern match is map unit Zo36–2a + Rd,Rc,Xk,Yh in hot subtropical desert around Lake Mackay and other alluvial and playa plains on the border of Northern Territory and Western Australia (Food and Agriculture Organization, 1978). At nearby Walungurru Airport, mean annual temperature is 26.2°C and mean annual precipitation is 280 mm (Bureau of Meteorology, 2020). The calcareous upper Moonlight Valley Tillite on the other hand has mainly Calcic Xerosols, in a map code Xk + Rc, most like Xk45–21 + Rc similar to the coastal plain inland of Eighty Mile Beach in the northwest coast of Australia (Food and Agriculture Organization, 1978). At nearby Mandora, mean annual temperature is 26.8°C and mean annual precipitation is 378 mm (Bureau of Meteorology, 2020). Both these places are in Western Australia within 800 km of Lake Argyle.

Similar soils also form in cooler climates. Hypercalcic Calcarosols similar to Galadil paleosols have formed on an alluvial plain near Clare, South Australia, under mean annual precipitation of 444 mm, and mean annual temperature of 15.2°C (profile CA7 of McKenzie *et al.*, 2004). Red Sodosols similar to Thamberalg paleosols formed on an alluvial plain near Deniliquin, New South Wales, under a mean annual precipitation of 339 mm and mean annual temperature of 15.7°C (profile SO3 of McKenzie *et al.*, 2004).

Original parent material

Parent materials to the paleosols were of two distinct kinds: dolomitic sandstones in the upper Moonlight Valley Tillite and basal Ranford Formation, and reworked felsic tuffs in the middle Ranford Formation zebra rock quarries. Silt size dolomite is as much as 24.4 vol% of parent materials to Jilam and Galadil profiles and was a conspicuous part of their loessic parent materials. A likely source for dolomite is glacial erosion of the Mesoproterozoic (*ca* 1128 Ma), Bungle Bungle Dolomite, in glacial valleys that were the source of the Moonlight Valley Tillite to the north (Corkeron, 2008). This geologically diverse recycled orogen source of the Ranford Formation is also compatible with a relatively flat REE pattern (Figure 10) similar to post-Archean Australian sediment (Nance & Taylor, 1976), and detrital zircons largely of Mesoproterozoic age (2000–1000 Ma; Lan *et al.*, 2020). The basal Ediacaran Nuccaleena Formation of South Australia (Retallack, 2011) is a similar partly eolian deposit of dolomite, quartz and feldspar capping a thick red tillite. A modern analogue is the late Pleistocene Peoria Silt of North America, which has carbonate content of 42% at Vicksburg, Mississippi (Fisk, 1951), 32% at Cumback, Indiana (Ruhe & Olson, 1980), and 31% in core G56 in Illinois 80 km north of St Louis (Grimley *et al.*, 1998).

Table 1. Pedotypes and diagnosis for Ediacaran red beds of Western Australia.

Pedotype	Meaning	Diagnosis	USDA (Soil Survey Staff, 2014)	Food and Agriculture Organisation (1978)	Classic (Stace *et al.*, 1968)	Australian (Isbell, 1996)
Danggang	Red ochre	Red siltstone surface (A) over bedded sandstone or claystone breccia (C)	Fluvent	Dystric Fluvisol	Alluvial Soil	Stratic Rudosol
Galadil	White paint	Red sandstone with penetrating fractal structures (A) over red sandstone with micritic nodules (Bk)	Calcid	Calcic Xerosol	Red Desert Soil	Supracalcic Calcarosol
Jilam	ground	Red sandstone with 'old elephant skin' (A) over red bedded sandstone (C)	Psamment	Calcaric Regosol	Calcareous Sand	Arenic Rudosol
Thamberalg	star	Red-grey layered surface (A) over siltstone with gypsum rosettes (By)	Gypsid	Orthic Solonchak	Solonchak	Hypersalic Hydrosol
Wajing	rainbow	Red siltstone surface (A) red-grey spotted and banded siltstone 'zebra rock' (Bg)	Aquept	Dystric Gleysol	Non-calcic Brown Soil	Oxyaquic Hydrosol

Indigenous names pedotypes around Lake Argyle are from Mirriwoong language (Olawsky & Kofod, 2019) and for Warnum region from Gija language (Jarraggirrem, 2017).

Table 2 Interpretation of pedotypes for Ediacaran red beds of Western Australia.

Pedotype	Paleoclimate	Ecosystems	Parent materials	Paleo-topography	Time for formation (kyrs)
Danggang	Not diagnostic for climate	Microbial earth	Quartzo-feldspathic sand	Lake margin lunette	0.1–1.0
Galadil	Frigid (−2.5 ± 0.5°C, and −1.7 ± 0.5°C mean annual temperature), arid (289 mm ± 147 mean annual precipitation), seasonal (44 ± 22 mm mean annual range of precipitation)	Microbial earth with *Yangtzi-ramulus zhangi*	Quartz–dolomite sand	Well-drained floodplain	11–17 ± 1.8
Jilam	Not diagnostic for climate	*Rivularites repertus* microbial earth	Quartz–dolomite sand	Near stream levee	1.0–2.0
Thamberalg	Temperate (11.9 ± 0.5°C mean annual temperature), hyperarid (106 ± 129 mm and 109 ± 129 mm mean annual temperature)	Microbial earth	Quartzo-feldspathic silt	Playa lake	89–97 ± 15
Wajing	Not diagnostic for climate	Microbial earth	Rhyolitic crystal tuff	Seasonally waterlogged floodplain	1.0–2.0

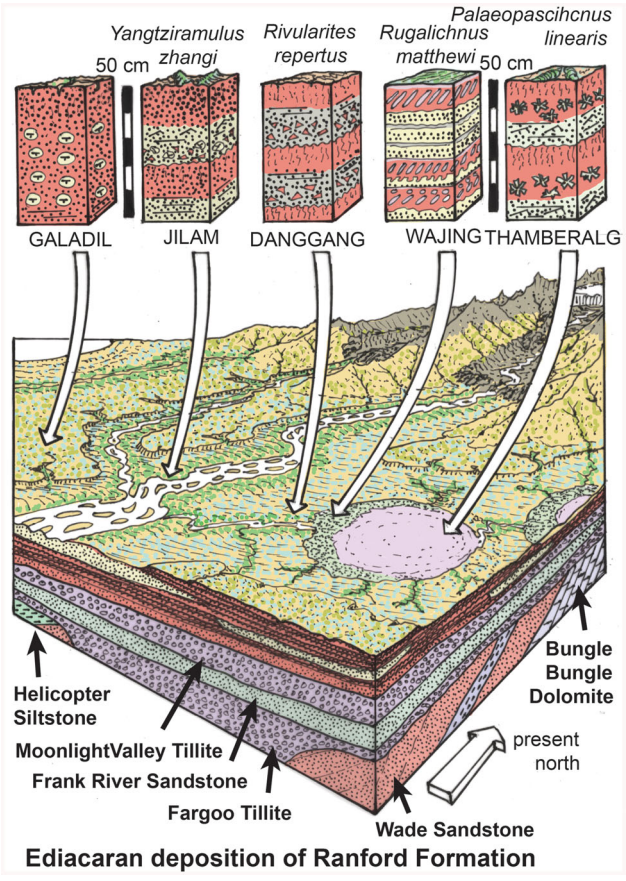

Figure 12. Reconstructed early Ediacaran soils of north Western Australia.

Two of the zebra rock beds studied are mica-rich, but one is mica-poor, and all are relatively massive beds compared with laminated to varved enclosing rocks of the Johnny Cake Member of the Ranford Formation. These zebra rock profiles may have been weathered from biotite tuffs and feldspathic tuffs. The tuffs are andesitic in the alkali/silica discrimination of Le Bas *et al.* (1986), but that composition is compromised by weathering in place (Loughnan & Roberts, 1990). Immobile trace element ratios of Zr/TiO_2 *vs* Nb/Y ratios of Winchester and Floyd (1977) are a better indication and are rhyolitic. No local active volcano is known; perhaps they were far-travelled airfall ash from 600 Ma volcanic arcs reconstructed to the west in what is now southern China (Scotese, 2009).

Reconstructed sedimentary setting

Two distinct sedimentary settings are represented by dolomitic sandstones of the upper Moonlight Valley Tillite and lower Jarrad Member, and zebra rock shales of the Johnny Cake Member of the Ranford Formation. Fluvial paleochannels (Facies TC) of dolomitic sandstone are capped by both Jilam and Galadil paleosols (Facies RS), and both paleosols are capped by fine-grained eolian siltstones (Facies IR). Galadil profiles are deeper and have large nodules as indications of greater time for formation (Retallack, 2005) and good drainage in infrequently flooded plains or terraces. In contrast, Jilam profiles are thin and grey at the base, as if waterlogged by groundwater (Vepraskas & Sprecher, 1997). Thus, Jilam profiles formed on alluvial levees.

Laminated and varved shales of the Johnny Cake Member represent a different sedimentary facies (RG) of varved and laminated, red and green, shales, with thin sandstones and weathered tuffs of a lacustrine basin that was intermittently exposed like modern playas and salt lakes (Benison *et al.*, 2007; Benison & Bowen, 2015). Thamberalg profiles with gypsum sand crystals are similar to dry lake Gypsids or Solonchak soils (McKenzie *et al.*, 2004). Zebra rock (Wajing) profiles were rhyolitic feldspar and biotite tuffs with poorly drained lower horizons within the lake basins, and show acid sulfate weathering (Loughnan & Roberts, 1990). Red sandstone Danggang profiles were on local sandy soils, perhaps eolian lunettes which commonly flank playa lakes (Bowler, 1973; Fitzsimmons *et al.*, 2014). Zebra rock's intimate admixture of oxidised and gleyed areas with open system enrichment and depletion of iron over small distances, but with red at the top and grey at the bottom, is similar to soils within the zone of seasonal rise and fall of water-table (Vepraskas & Sprecher, 1997).

Time for formation

Duration of soil formation for Galadil and Thamberalg pedotypes can be calculated from chronofunctions for modern arid land soils. Diameter of pedogenic carbonate nodules (D in cm) is related to radiocarbon age of nodules (A in kyrs) near Las Cruces, New Mexico, with modest precision ($r^2 = 0.57$, s.e. $= \pm 1.8$ kyr, $p = 0.001$), as follows (Retallack, 2005).

$$A = 3.92D^{0.34} \quad (4)$$

Similarly, abundance of gypsum in a profile (G as percentage surface area using comparison chart of Terry & Chilingar, 1955) is a metric for age (A in kyrs) in the Negev Desert of Israel, with fair precision ($r^2 = 0.95$, s.e. $= \pm 15$, and $p < 0.01$), as follows (Retallack, 2013).

$$A = 3.987G + 5.774 \quad (5)$$

The calcic chronofunction applied to five Galadil paleosols gives durations of $11-17 \pm 1.8$ kyr (13.9 ± 3.4 kyr mean and standard deviation), and the gypsic chronofunction applied to two Thamberalg profiles with 23 and 21% gypsum (Figure 4d) give durations of 97.4 ± 15 and 89.5 ± 15 kyr. These Ediacaran paleosols are thus strongly developed, on a scale in which Holocene (*ca* 10 ka) soils are moderately developed.

Other paleosols would have been much less developed, with a few millennia likely for Jilam and Wajing paleosols with sedimentary structures obscured to a depth of 15 cm, and only a century or less for Danggang paleosols with clear relict bedding. These are maximal estimates, because

they were derived by comparison with homogenisation of bedding in Pleistocene soils of the San Joaquin Valley, California (Harden, 1982), which were more actively rooted and burrowed than likely for Ediacaran soils.

Paleoclimate

Gypsic and calcic horizons are today found at depths in soils proportional to mean annual precipitation (Retallack, 2005, 2012b; Retallack & Huang, 2010), and this in turn is related to the balance between atmospheric CO_2 and soil CO_2 from terrestrial productivity (Breecker & Retallack, 2014). Comparisons of paleoclimatic inferences from Bk and By metrics with independent geochemical proxies do not show serious divergence in Neoproterozoic paleosols (Retallack, 2011, 2013; Retallack & Mindszenty, 1994), but Paleoproterozoic and Archean paleosols are problematic because of aggressive acid sulfate weathering (Retallack & Mao, 2019; Retallack *et al.*, 2016). Weathering by strong sulfuric acid rather than weak carbonic acid also affected Thamberalg and Wajing paleosols of the Ranford Formation, and explains their unusually high degree of chemical weathering (Loughnan & Roberts, 1990). Calcic soils are widespread, but gypsic soils form in extreme deserts such as the Atacama Desert of Chile (Ewing *et al.*, 2008; Navarro-González *et al.*, 2003). For calcic paleosols, mean annual precipitation (P in millimetres) is related to depth in the profile to calcareous nodules (D in cm corrected for burial compaction by equation 1) from a global compilation ($r^2 = 0.52$, s.e. = ±147, and $p < 0.0001$), as follows (Retallack, 2005).

$$P = 137.24 + 6.45D - 0.0132D^2 \quad (6)$$

For gypsic soils, another global compilation gives mean annual precipitation from depth to gypsum (D again compaction corrected: $r^2 = 0.63$, s.e. = ±129, and $p < 0.000000001$), as follows (Retallack & Huang, 2010).

$$P = 87.593e^{0.0209D} \quad (7)$$

Seasonality of precipitation, defined as wettest minus driest month mean precipitation (M in millimetres) is a function of thickness of the calcic horizon (T in cm), again from a global compilation (r^2=0.58, s.e. = ± 22, and $p < 0.00001$) as follows (Retallack, 2005).

$$R = 0.79T + 13.7 \quad (8)$$

Application of these Bk metrics to five Galadil paleosols of the upper Moonlight Valley Tillite and Jarrad Member of the Ranford Formation gives mean annual precipitation averaging 289 mm ± 147 (265–325 mm). Mean annual range of precipitation averaged 44 ± 22 (37–48 mm), which is seasonality much less than from modern monsoonal climates (Retallack, 2005).

Application of By metrics to two Thamberalg profiles give mean annual precipitation of 106 ± 129 mm and 109 ± 129 mm, which is hyperarid like the modern Atacama Desert (Ewing *et al.*, 2008; Navarro-González *et al.*, 2003).

Pedogenic paleothermometers based on soils of modern woody vegetation (Gallagher & Sheldon, 2013; Nordt & Driese, 2010; Sheldon *et al.*, 2002) are not applicable to likely microbial earths of Precambrian paleosols (Retallack & Mao, 2019). A paleothermometer based on modern soils under lichen-shrub tundra vegetation of Iceland (Óskarsson *et al.*, 2012) is an option, predicting temperature (T in °C) from chemical index of weathering (W in mole fractions) of non-calcareous Bw and By horizons ($r^2 = 0.81$, s.e. = 0.5, $p < 0.001$).

$$T = 0.21W - 8.93 \quad (9)$$

$$W = \frac{100Al_2O_3}{(Al_2O_3 + CaO + Na_2O)} \quad (10)$$

Another useful climofunction is the molar alkali index (I) of Sheldon *et al.* (2002), which includes desert soils in its training set, and gives temperature (T in °C) following equations 11 ($r^2 = 0.37$, s.e. = 4.4, $p < 0.00001$) and 12.

$$T = 18.5I + 17.3 \quad (11)$$

$$I = \frac{K_2O + Na_2O}{Al_2O_3} \quad (12)$$

This CIW proxy of Óskarsson *et al.* (2012) gives mean annual temperature of −2.5 ± 0.5°C for the upper Bk horizon of the Galadil silt loam and −1.7 ± 0.5°C for the upper Bk horizon of the Galadil sandy clay loam, which are frigid climates, evidently persisting above deposition of the tillite, as in the basal Ediacaran Nuccaleena Formation in South Australia (Retallack, 2011). These results are not disqualified by high content of lime (3–6 wt% CaO in Galadil profiles), specifically excluded for the similar chemical index of alteration (Nesbitt & Young, 1982, 1989), because the Icelandic training set for this paleothermometer also has high lime (3–11 wt%); however, in Iceland the lime is in volcanic glass rather than dolomite (Óskarsson *et al.*, 2012). This CIW metric also gave 11.9 ± 0.5°C for the Thamberalg profile. The alkali index proxy gave mean annual temperatures of 12.0 ± 4.4°C and 12.4 ± 4.4°C for the Galadil paleosols (respectively) and 16.9 ± 4.4°C for the Thamberalg profile. Paleotemperature was not calculated for Wajing paleosols also analysed because they were waterlogged (see above), and so did not reflect atmospheric temperatures.

Cool temperate to frigid paleotemperatures are surprising considering the low paleolatitude of these formations from paleomagnetic data. An average of eight paleolatitudes determined for zebra rock is 10° ± 6°, although one near-polar paleolatitude of 86° was also found by Abrajevitch *et al.* (2018) and may be a Paleozoic overprint. Ediacaran periglacial paleosols (Retallack, 2011, 2013) and tillites such as the Gaskiers Formation of Canada (Pu *et al.*, 2016) demonstrate that the Ediacaran Period was not a full recovery from extreme glacial conditions of the Cryogenian Snowball Earth (Hoffman *et al.*, 1998; Retallack, 2011).

Life on land

Two Ediacaran megafossils were found in the Upper Moonlight Valley Tillite and Ranford Formation, *Palaeopascichnus linearis* (Hawco *et al.*, 2019; Lan & Chen, 2012), and *Yangtziramulus zhangi* (Shen *et al.*, 2009). *Yangtziramulus* is a large fractally branching structure (Figure 5e) with vertical partitions reaching deeply into the substrate and defining large chambers filled with sediment (Figure 5f, g). *Yangtziramulus* has been considered a 'diagenetic structure, possibly mediated by microbial activity' (Conway Morris, 2006), and is similar to the more orthogonal peaked stromatolite *Thyssagites* (Walter, 1976). In both the Chinese and Australian specimens, the body partitions are encrusted with carbonate that extend deep below the surface. *Yangtziramulus* has irregular fractal architecture also generally similar to less-peaked *Fractofusus* (Gehling & Narbonne, 2007) and *Beothukis* (Taylor *et al.*, 2019). Similarly, it may have been an extinct organism of uncertain affinity within Class Vendobionta, variously interpreted as microbial colonies, xenophyophoran foraminifers, fungi, lichens, sponges, cnidarians, bilaterians, or stem metazoan (Retallack & Broz, 2020). In the Ediacaran Shibantan Member of the Denying Formation in China, *Yangtziramulus* was regarded as a shallow subtidal sediment binder (Shen *et al.*, 2009), but intertidal paleosols with oxidised surfaces (A horizon) and gleyed pyritic subsurface (Bg) horizons have been observed in the Shibantan Member (Retallack, 2014). Other evidence for intertidal or supratidal exposure of some horizons of the Shibantan Member comes from strong correlation of $\delta^{18}O$ and $\delta^{13}C$ values of its carbonates (as in Figure 10a, b), and a divergent mix of local oxic (low Fe and Mn, Ce/Ce*, Y/Ho, V/Cr) and anoxic [V/Sc, Ni/Co–, V/(V + Ni)] chemical indicators (Duda *et al.*, 2014; Wan *et al.,* 2020). In contrast, *Yangtziramulus* in the upper Moonlight Valley Tillite (Figure 5e–g) is on the surface of red Galadil paleosols, suggesting that it may have been a supratidal or terrestrial organism.

In the Donkey Creek outcrop of the Ranford Formation (Figure 6b), Lan and Chen (2012) reported *Palaeopascichnus* sp. indet, which can now be identified as *Palaeopaschichnus linearis* (Kolesnikov *et al.*, 2018). At first *Palaeopascichnus* was interpreted as a meandering trail trace fossil (Glaessner, 1969; Parcha & Pandey, 2011), alga (Haines, 2000), faecal string (Jensen, 2003), stratiform stromatolite (Runnegar, 1995), or xenophyophore foraminifer (Kolesnikov *et al.*, 2018; Seilacher *et al.*, 2003), but recent work has largely concluded that it was a chambered protozoan body fossil, distinct from modern xenophyophores (Antcliffe *et al.*, 2011; Dong *et al.*, 2008; Gehling & Droser, 2009; Hawco *et al.*, 2019). *Palaeopascichnus* has been widely assumed to have been marine (Antcliffe *et al.*, 2011; Hawco *et al.*, 2019), and the species *P. delicatus* had a boron content compatible either with marine or terrestrial salt lakes (Retallack, 2020). In the Ranford Formation, *Palaeopascichnus* is in the same sequence as Thamberalg paleosols of hypersaline playa lakes (Figure 6b), but in lacustrine sediments rather than in the paleosols.

A variety of fossils and MISS are known from the Ranford Formation and upper Moonlight Valley Tillite (Lan & Chen, 2012, 2013). Some of these from the Ranford Formation are ridged surfaces with disconnected fragments (Figure 4e), comparable with aquatic microbial mats and the trace fossils *Rugalichnus matthewi* (Stimson *et al.*, 2017). These undulose fabrics contrast with surfaces from the upper Moonlight Valley Tillite showing a patchwork of cracking and healing called 'old elephant skin' or *Rivularites repertus* (Retallack, 2013; Retallack & Broz, 2020). 'Old elephant skin' refers to a complex pattern of cracks, but there is also evidence of push-up ridges and domes, and thus alternating tension and compression. These textures are identical to surfaces of biological soil crusts (Belnap, 2003) and microbial earths (Figure 11d).

Finally, there is chemical and petrographic evidence for life in these paleosols. Thin-sections show lack of lamination in paleosol surface horizons (Figures 3 and 5f, g), perhaps owing to vertical thread-forming microbial consortia (Retallack, 2012a). All the paleosols also show significant loss of phosphorus (Figure 8), another indication of a microbial earth soil (Neaman *et al.*, 2005a, 2005b).

Conclusions

Ediacaran paleoenvironments and paleosols of the Ranford Formation are reconstructed in Figure 12. This study outlines diagnostic paleosol criteria of pedogenic cracking patterns, sand crystals, interflag sandstone laminae, mineral weathering trends, chemical weathering trends, tau analysis, stable isotopic correlation and biotic microstructures. Once paleosols are recognised implying formation within the critical zone transitional between earth and air, their ancient environments may be interpreted. The enigmatic ornamental zebra rock can now be seen as a lowland seasonally waterlogged, redoximorphic soil (Wajing pedotype). Ediacaran paleosols of north Western Australia are evidence of arid and cool to cold temperate climates. Paleosols also reveal landscapes with moderately developed soils and stable ecosystems, as well as weakly developed and early successional soils and communities. These communities of scattered, ground-hugging, sessile large organisms would have appeared similar to modern polsterlands of alpine, polar and extreme deserts.

Acknowledgements

Bruce Runnegar, Shuhai Xiao, Natalia Bykova and Dima Grazhdankin offered useful discussion. Brian and Jo Fennell generously provided illustrations and slabs of Snappy Gum Ridge zebra rock, and access to their quarry on Donkey Creek. Ruth Duncan generously offered a tour of the Duncan Road quarry, and permission to collect there. I am grateful for helpful reviews from Paul Carr and an anonymous reviewer.

Disclosure statement

No potential conflict of interest was reported by the author(s).

Data availability statement

Supplementary data that support the findings of this study are openly available from the University of Oregon at https://doi.org/10.7910/DVN/OXAFZI

References

Abrajevitch, A., Pillans, B. J., Roberts, A. P., & Kodama, K. (2018). Magnetic properties and paleomagnetism of Zebra Rock, Western Australia: Chemical remanence acquisition in hematite pigment and Ediacaran geomagnetic field behavior. *Geochemistry, Geophysics, Geosystems*, *19*(3), 732–748. https://doi.org/10.1002/2017GC007091

Aiello, I. W., Garrison, R. E., Moore, E. C., Kastner, M., & Stakes, D. S. (2001). Anatomy and origin of carbonate structures in a Miocene cold-seep field. *Geology*, *29*(12), 1111–1114. https://doi.org/10.1130/0091-7613(2001)0291111:AAOOCS2.0.CO;2

Almohandis, A. A. (2002). Mineralogy and chemistry of desert roses, Ayn Dar area, Abqaiq, eastern province, Saudi Arabia. *Qatar University Science Journal*, *22*, 191–204. http://hdl.handle.net/10576/9660

Álvaro, J. J., Van Vliet-Lanoë, B., Vennin, E., & Blanc-Valleron, M. M. (2003). Lower Cambrian paleosols from the Cantabrian Mountains (northern Spain): A comparison with Neogene–Quaternary estuarine analogues. *Sedimentary Geology*, *163*(1–2), 67–84. https://doi.org/10.1016/S0037-0738(03)00159-3

Antcliffe, J. B., Gooday, A. J., & Brasier, M. D. (2011). Testing the protozoan hypothesis for Ediacaran fossils: A developmental analysis of *Palaeopascichnus*. *Palaeontology*, *54*(5), 1157–1175. https://doi.org/10.1111/j.1475-4983.2011.01058.x

Bao, H., Chen, Z. Q., & Zhou, C. (2012). An ^{17}O record of late Neoproterozoic glaciation in the Kimberley region, Western Australia. *Precambrian Research*, *216-219*(1), 152–161. https://doi.org/10.1016/j.precamres.2012.06.019

Barbour, M. M., & Farquhar, G. D. (2000). Relative humidity- and ABA-induced variation in carbon and oxygen isotope ratios of cotton leaves. *Plant, Cell & Environment*, *23*(5), 473–485. https://doi.org/10.1046/j.1365-3040.2000.00575.x

Barbour, M. M., Walcroft, A. S., & Farquhar, G. D. (2002). Seasonal variation in $\delta^{13}C$ and $\delta^{18}O$ of cellulose from growth rings of *Pinus radiata*. *Plant, Cell and Environment*, *25*(11), 1483–1499. https://doi.org/10.1046/j.0016-8025.2002.00931.x

Bavinton, O. A., & Taylor, S. R. (1980). Rare earth element geochemistry of Archean metasedimentary rocks from Kambalda, Western Australia. *Geochimica et Cosmochimica Acta*, *44*(5), 639–648. https://doi.org/10.1016/0016-7037(80)90154-4

Belnap, J. (2003). Comparative structure of physical and biological soil crusts. In. J. Belnap & O. L. Lange (Eds.), *Biological soil crusts: Structure, function and management* (pp. 177–191). Springer.

Benison, K. C., & Bowen, B. B. (2015). The evolution of end-member continental waters: The origin of acidity in southern Western Australia. *GSA Today*, *25*(6), 4–10. https://doi.org/10.1130/GSATG231A.1

Benison, K. C., Bowen, B. B., Oboh-Ikuenobe, F. E., Jagniecki, E. A., LaClair, D. A., Story, S. L., Mormile, M. R., & Hong, B. Y. (2007). Sedimentology of acid saline lakes in southern Western Australia: Newly described processes and products of an extreme environment. *Journal of Sedimentary Research*, *77*(5), 366–388. https://doi.org/10.2110/jsr.2007.038

Bestland, E. A., Retallack, G. J., Rice, A. E., & Mindszenty, A. (1996). Late Eocene detrital laterites in central Oregon: Mass balance geochemistry, depositional setting and landscape evolution. *Geological Society of America Bulletin*, *108*(3), 285–302. https://doi.org/10.1130/0016-7606(1996)1080285:LEDLIC2.3.CO;2

Bindeman, I. N., Eiler, J. M., Wing, B. A., & Farquhar, J. (2007). Rare sulfur and triple oxygen isotope geochemistry of volcanogenic sulfate aerosols. *Geochimica et Cosmochimica Acta*, *71*(9), 2326–2343. https://doi.org/10.1016/j.gca.2007.01.026

Boas, J. F., Cashion, J. D., Chadwick, J., Clark, M. J., Mackie, R. D., & Mattievich, E. (2005). Electron paramagnetic resonance of defects and Fe^{3+} in Kimberley Zebra Rock. *Abstracts of the National Congress of Australian Institute of Physics*, *16*, 268. http://aipcongress2005.anu.edu.au/pdf/AIPC_Handbook_V2.pdf

Bockheim, J. G., & Hartemink, A. E. (2013). Classification and distribution of soils with lamellae in the USA. *Geoderma*, *206*, 92–100. https://doi.org/10.1016/j.geoderma.2013.04.014

Bolhar, R., Van Kranendonk, M. J., & Kamber, B. S. (2005). A trace element study of siderite jasper banded iron formation in the 3.45 Ga Warrawoona Group, Pilbara Craton: Formation from hydrothermal fluids and shallow seawater. *Precambrian Research*, *137*(1–2), 93–114. https://doi.org/10.1016/j.precamres.2005.02.001

Bowler, J. M. (1973). Clay dunes: Their occurrence, formation and environmental significance. *Earth-Science Reviews*, *9*(4), 315–338. https://doi.org/10.1016/0012-8252(73)90001-9

Breecker, D. O., & Retallack, G. J. (2014). Refining the pedogenic carbonate atmospheric CO_2 proxy and application to Miocene CO_2. *Palaeogeography, Palaeoclimatology, Palaeoecology*, *406*, 1–8. https://doi.org/10.1016/j.palaeo.2014.04.012

Brimhall, G. H., Chadwick, O. A., Lewis, C. J., Compston, W., Williams, I. S., Danti, K. J., Dietrich, W. E., Power, M. E., Hendricks, D., & Bratt, J. (1992). Deformational mass transport and invasive processes in soil evolution. *Science*, *255*(5045), 695–702. https://doi.org/10.1126/science.255.5045.695

Bureau of Meteorology. (2020). *Climate statistics for Australian locations*. Retrieved May 11, 2020, from http://www.bom.gov.au/climateaverages

Cant, D. J., & Walker, R. G. (1978). Fluvial processes and facies sequences in the sandy braided South Saskatchewan River, Canada. *Sedimentology*, *25*(5), 625–648. https://doi.org/10.1111/j.1365-3091.1978.tb00323.x

Chadwick, O. A., Brimhall, G. H., & Hendricks, D. M. (1990). From a black to a gray box—a mass balance interpretation of pedogenesis. *Geomorphology*, *3*(3–4), 369–390. https://doi.org/10.1016/0169-555X(90)90012-F

Chen, C., Barcellos, D., Richter, D. D., Schroeder, P. A., & Thompson, A. (2019). Redoximorphic Bt horizons of the Calhoun CZO soils exhibit depth-dependent iron-oxide crystallinity. *Journal of Soils and Sediments*, *19*(2), 785–797. https://doi.org/10.1007/s11368-018-2068-2

Clauer, N., O'Neil, J. R., Bonnnot-Courtois, C., & Holtzapfel, T. (1990). Morphological, chemical, and isotopic evidence for an early diagenetic evolution of detrital smectite in marine sediments. *Clays and Clay Minerals*, *38*(1), 33–46. https://doi.org/10.1346/CCMN.1990.0380105

Compton, J. S., White, R. A., & Smith, M. (2003). Rare earth element behavior in soils and salt pan sediments of a semi-arid granitic terrain in the Western Cape, South Africa. *Chemical Geology*, *201*(3–4), 239–255. https://doi.org/10.1016/S0009-2541(03)00239-0

Conway Morris, S. (2006). Darwin's dilemma: The realities of the Cambrian "explosion. *Philosophical Transactions of the Royal Society B: Biological Sciences*, *361*(1470), 1069–1083. https://doi.org/10.1098/rstb.2006.1846

Corkeron, M. (2007). 'Cap carbonates' and Neoproterozoic glacigenic successions from the Kimberley region. *Sedimentology*, *54*(4), 871–903. https://doi.org/10.1111/j.1365-3091.2007.00864.x

Corkeron, M. (2008). Deposition and palaeogeography of a glacigenic Neoproterozoic succession in the east Kimberley, Australia. *Sedimentary Geology*, *204*(3–4), 61–82. https://doi.org/10.1016/j.sedgeo.2007.12.010

de Sá Paye, H., de Mello, J. W., de Magalhães Mascarenhas, G. R. L., & Gasparon, M. (2016). Distribution and fractionation of the rare earth elements in Brazilian soils. *Journal of Geochemical Exploration*, *161*, 27–41. https://doi.org/10.1016/j.gexplo.2015.09.003

Dong, L., Xiao, S., Shen, B., & Zhou, C. (2008). Silicified *Horodyskia* and *Palaeopascichnus* from upper Ediacaran cherts in South China: Tentative phylogenetic interpretation and implications for evolutionary stasis. *Journal of the Geological Society*, *165*(1), 367–378. https://doi.org/10.1144/0016-76492007-074

Dow, D. B., & Gemuts, I. (1969). Geology of the Kimberley Region, Western Australia: The East Kimberley. *Bulletin of the Bureau of Mineral Resources Geology & Geophysics Canberra*, *106*, 135.

Draut, A. E., & Rubin, D. M. (2008). The role of eolian sediment in the preservation of archeologic sites along the Colorado River corridor in Grand Canyon National Park. *Arizona. U.S. Geological Survey Professional Paper*, *1756*, 1–71. https://doi.org/10.3133/pp1756

Draut, A. E., Rubin, D. M., Dierker, J. L., Fairley, H. C., Griffiths, R. E., Hazel, J. E., Hunter, R. E., Kohl, K., Leap, L. M., Nials, F. L., Topping, D. J., & Yeatts, M. (2008). Application of sedimentary-structure interpretation to geoarchaeological investigations in the Colorado River Corridor, Grand Canyon, Arizona, USA. *Geomorphology*, *101*(3), 497–509. https://doi.org/10.1016/j.geomorph.2007.04.032

Driese, S. G., Simpson, E. L., & Eriksson, K. A. (1995). Redoximorphic Paleosols in alluvial and lacustrine deposits, 1.8 Ga Lochness Formation, Mount Isa, Australia; pedogenic processes and implications for paleoclimate. *Journal of Sedimentary Research*, *65*(4a), 675–689. https://doi.org/10.1306/D4268199-2B26-11D7-8648000102C1865D

Duda, J. P., Blumenberg, M., Thiel, V., Simon, K., Zhu, M., & Reitner, J. (2014). Geobiology of a palaeoecosystem with Ediacara-type fossils: The Shibantan Member (Dengying Formation, South China). *Precambrian Research*, *255*, 48–62. https://doi.org/10.1016/j.precamres.2014.09.012

Dunnet, D. (1965). A new occurrence of Proterozoic 'jellyfish' from the Kimberley Region, Western Australia. *Report of the Bureau of Mineral Resources Geology and Geophysics, Canberra*, *134*, 5.

Ehleringer, J. R., Buchmann, N., & Flanagan, L. B. (2000). Carbon isotope ratios in belowground carbon cycle processes. *Ecological Applications*, *10*(2), 412–422.https://doi.org/10.1890/1051-0761(2000)010[0412:CIRIBC]2.0.CO;2

Ehleringer, J. R., & Cook, C. S. (1998). Carbon and oxygen isotope ratios of ecosystem respiration along an Oregon conifer transect: Preliminary observations based on small flask sampling. *Tree Physiology*, *18*(8–9), 513–519. https://doi.org/10.1093/treephys/18.8-9.513

Evins, L. Z., Jourdan, F., & Phillips, D. (2009). The Cambrian Kalkarindji large igneous province: Extent and characteristics based on new $^{40}Ar/^{39}Ar$ and geochemical data. *Lithos*, *110*(1–4), 294–304. https://doi.org/10.1016/j.lithos.2009.01.014

Ewing, S. A., Macalady, J. L., Warren-Rhodes, K., McKay, C. P., & Amundson, R. (2008). Changes in the soil C cycle at the arid-hyperarid transition in the Atacama Desert. *Journal of Geophysics Research Biogeosciences*, *113*(G2), G02S90. https://doi.org/10.1029/2007JG000495

Fisk, H. N. (1951). Loess and Quaternary geology of the Lower Mississippi Valley. *The Journal of Geology*, *59*(4), 333–356. https://doi.org/10.1086/625872

Fitzsimmons, K. E., Stern, N., & Murray-Wallace, C. V. (2014). Depositional history and archaeology of the central Lake Mungo lunette, Willandra Lakes, southeast Australia. *Journal of Archaeological Science*, *41*, 349–364. https://doi.org/10.1016/j.jas.2013.08.004

Foden, J. D., Nesbitt, R. W., & Rutland, R. W. R. (1984). The geochemistry and crustal origin of the Archaean acid intrusive rocks of the Agnew Dome, Lawlers, Western Australia. *Precambrian Research*, *23*(3–4), 247–271. https://doi.org/10.1016/0301-9268(84)90046-9

Food and Agriculture Organization. (1978). *Soil map of the World 1: 5,000,000. Vol. X. Australasia* (p. 21). UNESCO.

Frey, M. (1987). Very low grade metamorphism of clasticsedimentary rocks. In M. Frey (Ed.), *Low temperature metamorphism* (pp. 9–58). Blackie.

Gallagher, T. M., & Sheldon, N. D. (2013). A new paleothermometer for forest paleosols and its implications for Cenozoic climate. *Geology*, *41*(6), 647–650. https://doi.org/10.1130/G34074.1

Gariboldi, K., Gioncada, A., Bosio, G., Malinverno, E., Di Celma, C., Tinelli, C., Cantalamessa, G., Landini, W., Urbina, M., & Bianucci, G. (2015). The dolomite nodules enclosing fossil marine vertebrates in the East Pisco Basin, Peru: Field and petrographic insights into the Lagerstätte formation. *Palaeogeography, Palaeoclimatology, Palaeoecology*, *438*, 81–95. https://doi.org/10.1016/j.palaeo.2015.07.047

Gastaldo, R. A., Allent, G., & Huci, A. Y. (2009). The tidal character of fluvial sediments of the modern Mahakam River delta, Kalimantan, Indonesia. In B. W. Flemming (Ed.), *Tidal signatures in modern and ancient sediments* (Vol. 28, pp. 171–181). Special Publication of the International Association of Sedimentologists.

Gehling, J. G. (2000). Environmental interpretation and a sequence stratigraphic framework for the terminal Proterozoic Ediacara Member within the Rawnsley Quartzite, South Australia. *Precambrian Research*, *100*(1–3), 65–95. https://doi.org/10.1016/S0301-9268(99)00069-8

Gehling, J. G., & Droser, M. L. (2009). Textured organic surfaces associated with the Ediacara biota in South Australia. *Earth-Science Reviews*, *96*(3), 196–206. https://doi.org/10.1016/j.earscirev.2009.03.002

Gehling, J. G., & Narbonne, G. M. (2007). Spindle-shaped Ediacara fossils from the Mistaken Point assemblage, Avalon zone, Newfoundland. *Canadian Journal of Earth Sciences*, *44*(3), 367–387. https://doi.org/10.1139/e07-003

Geidans, L. (1981). Zebra rock of Western Australia. *Abstracts of the Geological Society of Australia*, *3*, 22.

Glaessner, M. F. (1969). Trace fossils from the Precambrian and basal Cambrian. *Lethaia*, *2*(4), 369–393. https://doi.org/10.1111/j.1502-3931.1969.tb01258.x

Grazhdankin, D. V., Goy, Y. Y., & Maslov, A. V. (2012). Late Riphean microbial colonies adapted to desiccating environments. *Doklady Earth Sciences*, *446*(2), 1157–1161. https://doi.org/10.1134/S1028334X12100157

Grey, K. (1981a). Proterozoic "jellyfish" from the Mount Brooking area, Lissadell Sheet, Kimberley region. *Geological Survey of Western Australia Palaeontology Report*, *29*, 1–4. https://dmpbookshop.eruditetechnologies.com.au/product/proterozoic-jellyfish-from-the-mount-brooking-area-lissadell-sheet-kimberley-region.do

Grey, K. (1981b). Additional samples of Proterozoic "jellyfish" from the Mount Brooking area, Lissadell Sheet, Kimberley region. *Geological Survey of Western Australia Palaeontology Report*, *52*, 1–2. https://dmpbookshop.eruditetechnologies.com.au/product/additional-samples-of-proterozoic-jellyfish-from-the-mount-brooking-area-lissadell-sheet-kimberley-region.do

Grey, K., & Corkeron, M. (1998). Late Neoproterozoic stromatolites in glacigenic successions of the Kimberley region, Western Australia: Evidence for a younger Marinoan glaciation. *Precambrian Research*, *92*(1), 65–87. https://doi.org/10.1016/S0301-9268(98)00068-0

Grimley, D. A., Follmer, L. R., & McKay, E. D. (1998). Magnetic susceptibility and mineral zonation controlled by provenance in loess along the Illinois and central Mississippi Valley. *Quaternary Research*, *49*(1), 24–36. https://doi.org/10.1006/qres.1997.1947

Haines, P. W. (2000). Problematic fossils in the late Neoproterozoic Wonoka Formation, South Australia. *Precambrian Research*, *100*(1–3), 97–108. https://doi.org/10.1016/S0301-9268(99)00070-4

Harden, J. W. (1982). A quantitative index of soil development from field descriptions: Examples from a chronosequence in central California. *Geoderma*, *28*(1), 1–28. https://doi.org/10.1016/0016-7061(82)90037-4

Hawco, J. B., Kenchington, C. G., & McIlroy, D. (2019). A quantitative and statistical discrimination of morphotaxa within the Ediacaran

genus *Palaeopascichnus*. *Papers in Palaeontology*. https://doi.org/10.1002/spp2.1290

Hayes, J. L., Riebe, C. S., Holbrook, S. W., Flinchum, B. A., & Hartsough, P. C. (2019). Porosity production in weathered rock: Where volumetric strain dominates over chemical mass loss. *Science Advances*, *5*(9), eaao0834. https://doi.org/10.1126/sciadv.aao0834

Hebert, C. L., Kaufman, A. J., Penniston-Dorland, S. C., & Martin, A. J. (2010). Radiometric and stratigraphic constraints on terminal Ediacaran (post-Gaskiers) glaciation and metazoan evolution. *Precambrian Research*, *182*(4), 402–412. https://doi.org/10.1016/j.precamres.2010.07.008

Hobson, R. A. (1930). Zebra rock from Kimberley. *Journal of the Royal Society of Western Australia*, *16*, 57–70.

Hoffman, P. F., Kaufman, A. J., Halverson, G. P., & Schrag, D. P. (1998). A Neoproterozoic Snowball Earth. *Science*, *281*(5381), 1342–1346. https://doi.org/10.1126/science.281.5381.1342

Huang, C-M., Wang, C-S., & Tang, Y. (2005). Stable carbon and oxygen isotopes of pedogenic carbonates in Ustic Vertisols: Implications for paleoenvironmental change. *Pedosphere*, *15*(4), 539–544.

Hunter, R. E. (1977). Basic types of stratification in small eolian dunes. *Sedimentology*, *24*(3), 361–387. https://doi.org/10.1111/j.1365-3091.1977.tb00128.x

Isbell, R. F. (1996). *The Australian soil classification* (revised ed., pp. 144). CSIRO Publishing.

Jafarzadeh, A. A., & Burnham, C. P. (1992). Gypsum crystals in soils. *Journal of Soil Science*, *43*(3), 409–420. https://doi.org/10.1111/j.1365-2389.1992.tb00147.x

Jarraggirrem. (2017). *Gija-English online dictionary*. Retrieved May 28, 2020, from https://issuu.com/jarraggirrem/docs/gija-english-dictionary

Jensen, S. (2003). The Proterozoic and Earliest Cambrian trace fossil record: Patterns, problems, and perspectives. *Integrative and Comparative Biology*, *43*(1), 219–228. https://doi.org/10.1093/icb/43.1.219

Jourdan, F., Hodges, K., Sell, B., Schaltegger, U., Wingate, M. T. D., Evins, L. Z., Söderlund, U., Haines, P. W., Phillips, D., & Blenkinsop, T. (2014). High-precision dating of the Kalkarindji large igneous province, Australia, and synchrony with the Early–Middle Cambrian (Stage 4–5) extinction. *Geology*, *42*(6), 543–546. https://doi.org/10.1130/G35434.1

Kelka, U., Veveakis, M., Koehn, D., & Beaudoin, N. (2017). Zebra rocks: Compaction waves create ore deposits. *Scientific Reports*, *7*(1), 1–9. https://doi.org/10.1038/s41598-017-14541-3

Kennedy, M. J. (1996). Stratigraphy, sedimentology, and isotopic geochemistry of Australian Neoproterozoic postglacial cap dolostones; deglaciation, $\delta^{13}C$ excursions, and carbonate precipitation. *Journal of Sedimentary Research*, *66*(6), 1050–1064. https://doi.org/10.2110/jsr.66.1050

Knauth, L. P., Brilli, M., & Klonowski, S. (2003). Isotope geochemistry of caliche developed on basalt. *Geochimica et Cosmochimica Acta*, *67*(2), 185–195. https://doi.org/10.1016/S0016-7037(02)01051-7

Knoll, A., Walter, M., Narbonne, G., & Christie-Blick, N. (2006). The Ediacaran Period: A new addition to the geologic time scale. *Lethaia*, *39*(1), 13–30. https://doi.org/10.1080/00241160500409223

Kolesnikov, A. V., Rogov, V. I., Bykova, N. V., Danelian, T., Clausen, S., Maslov, A. V., & Grazhdankin, D. V. (2018). The oldest skeletal macroscopic organism *Palaeopascichnus linearis*. *Precambrian Research*, *316*, 24–37. https://doi.org/10.1016/j.precamres.2018.07.017

Kruse, P. D., Laurie, J. R., & Webby, B. D. (2004). Cambrian geology and palaeontology of the Ord Basin. *Memoirs of the Association of Australasian Palaeontologists*, *30*, 1–58. http://hdl.handle.net/1959.14/41350

Kurtz, A. C., Derry, L. A., & Chadwick, O. A. (2001). Accretion of Asian dust to Hawaiian soils: Isotopic, elemental, and mineral mass balances. *Geochimica et Cosmochimica Acta*, *65*(12), 1971–1983. https://doi.org/10.1016/S0016-7037(01)00575-0

Lan, Z. W., & Chen, Z. Q. (2012). Possible animal body fossils from the late Neoproterozoic interglacial successions in the Kimberley region, northwestern Australia. *Gondwana Research*, *21*(1), 293–301. https://doi.org/10.1016/j.gr.2011.05.014

Lan, Z. W., & Chen, Z. Q. (2013). Proliferation of MISS-forming microbial mats after the late Neoproterozoic glaciations: Evidence from the Kimberley region, NW Australia. *Precambrian Research*, *224*, 529–550. https://doi.org/10.1016/j.precamres.2012.11.008

Lan, Z. Q., Zhang, S., Li, X. H., Pandey, S. K., Sharma, M., Shukla, Y., Ahmad, S., Sarkar, S., & Zhai, M. (2020). Towards resolving the 'jigsaw puzzle' and age-fossil inconsistency within East Gondwana. *Precambrian Research*, *345*, 105775. https://doi.org/10.1016/j.precamres.2020.105775

Larcombe, C. O. G. (1927). Some rocks from four miles east of Argyle Station, Ord River, King district, Kimberley division. *Annual Progress Report of the Geological Survey of Western Australia, for 1926*, 23–24. https://www.dmp.wa.gov.au/Documents/About-Us-Careers/AnnualReport_1926.pdf

Larcombe, C. O. G. (1925). *Rock specimens from Ord River and Oakover River respectively*. Annual Progress Report of the Geological Survey of Western Australia, for 1924 (Vol. 19). Geological Survey of Western Australia.

Bas, M. J. L., Maitre, R. W. L., Streckeisen, A., & Zanettin, B. (1986). A chemical classification of volcanic rocks based on the total alkali-silica diagram. *Journal of Petrology*, *27*(3), 745–750. https://doi.org/10.1093/petrology/27.3.745

Liivamägi, S., Somelar, P., Mahaney, W. C., Kirs, J., Vircava, I., & Kirsimäe, K. (2014). Late Neoproterozoic Baltic paleosol: Intense weathering at high latitude? *Geology*, *42*(4), 323–326. https://doi.org/10.1130/G35209.1

Lohmann, K. G. (1988). Geochemical patterns of meteoric diagenetic systems and their application to studies of paleokarst. In N. P. James & P. W. Choquette (Eds.), *Paleokarst* (pp. 59–80). Springer.

Loughnan, F. C., & Roberts, F. I. (1990). Composition and origin of the 'zebra rock' from the East Kimberley region of Western Australia. *Australian Journal of Earth Sciences*, *37*(2), 201–205. https://doi.org/10.1080/08120099008727920

Ludvigson, G. A., González, L. A., Fowle, D. A., Roberts, J. A., Driese, S. G., Villarreal, M. A., Smith, J. J., Suarez, M. B., & Nordt, L. C. (2013). Paleoclimatic applications and modern process studies of pedogenic siderite. In S. G. Driese & L. C. Nordt (Eds.), *New Frontiers in Paleopedology and Terrestrial Paleoclimatology* (pp. 79–87, Vol. 104). Society of Economic Paleontologists & Mineralogists Special Publication.

Ludvigson, G. A., González, L. A., Metzger, R. A., Witzke, B. J., Brenner, R. L., Murillo, A. P., & White, T. S. (1998). Meteoric sphaerosiderite lines and their use for paleohydrology and paleoclimatology. *Geology*, *26*(11), 1039–1042. https://doi.org/10.1130/0091-7613(1998)026<1039:MSLATU>2.3.CO;2

Marshall, P. E., Widdowson, M., & Murphy, D. T. (2016). The Giant Lavas of Kalkarindji: Rubbly pāhoehoe lava in an ancient continental flood basalt province. *Palaeogeography, Palaeoclimatology, Palaeoecology*, *441*, 22–37. https://doi.org/10.1016/j.palaeo.2015.05.006

Martin, E., & Bindeman, I. (2009). Mass-independent isotopic signatures of volcanic sulfate from three supereruption ash deposits in Lake Tecopa, California. *Earth and Planetary Science Letters*, *282*(1–4), 102–114. https://doi.org/10.1016/j.epsl.2009.03.005

Mattievich, E., Chadwick, J., Cashion, J. D., Boas, J. F., Clark, M. J., Mackie, R. D. (2003). *Macroscopic ferronematic liquid crystals determine the structure of Kimberley Zebra Rock* [Paper presentation]. Conference Handbook Annual Condensed Matter Physics Meeting Wagga, Wagga, 27, 1–3. http://www.aip.org.au/wp-content/uploads/cmm/2003/WW03_33.pdf

Mawson, D., & Segnit, E. R. (1949). Purple slates of the Adelaide System. *Transactions of the Royal Society of South Australia*, *72*, 276–280.

McKenzie, N., Jacquier, D., Isbale, R., & Brown, K. (2004). *Australian soils and landscapes* (p. 416). CSIRO.

Mehmood, M., Yaseen, M., Khan, E. U., & Khan, M. J. (2018). Dolomite and dolomitization model—a short review. *International Journal of Hydrology*, *2*(5), 549–553. https://doi.org/10.15406/ijh.2018.02.00124

Melim, L. A., Swart, P. K., & Eberli, G. P. (2004). Mixing zone diagenesis in the subsurface of Florida and the Bahamas. *Journal of Sedimentary Research*, *74*(6), 904–913. https://doi.org/10.1306/042904740904

Mory, A. J., & Beere, G. M. (1985). Palaeozoic stratigraphy of the Ord Basin, Western Australia and Northern Territory. *Geological Survey of Western Australia Reports*, *14*, 36–45. https://dmpbookshop.eruditetechnologies.com.au//product/Palaeozoic-stratigraphy-of-the-Ord-Basin-Western-Australia-and-Northern-Territory.do

Murphy, C. P. (1983). Point counting pores and illuvial clay in thin section. *Geoderma*, *31*(2), 133–150. https://doi.org/10.1016/0016-7061(83)90004-6

Nance, W. B., & Taylor, S. R. (1976). Rare earth element patterns and crustal evolution—I. Australian post-Archean sedimentary rocks. *Geochimica et Cosmochimica Acta*, *40*(12), 1539–1551. https://doi.org/10.1016/0016-7037(76)90093-4

Navarro-González, R., Rainey, F. A., Molina, P., Bagaley, D. R., Hollen, B. J., de la Rosa, J., Small, A. M., Quinn, R. C., Grunthaner, F. J., Cáceres, L., Gomez-Silva, B., & McKay, C. P. (2003). Mars-like soils in the Atacama Desert, Chile, and the dry limit of microbial life. *Science (New York, N.Y.)*, *302*(5647), 1018–1021. https://doi.org/10.1126/science.1089143

Neaman, A., Chorover, J., & Brantley, S. L. (2005a). Element mobility patterns record organic ligands in soils on early Earth. *Geology*, *33*(2), 117–120. https://doi.org/10.1130/G20687.1

Neaman, A., Chorover, J., & Brantley, S. L. (2005b). Implications of the evolution of organic acid moieties for basalt weathering over geological time. *American Journal of Science*, *305*(2), 147–185. https://doi.org/10.2475/ajs.305.2.147

Nesbitt, H. W., & Young, G. M. (1982). Early Proterozoic climates and plate motions inferred from major element chemistry of lutites. *Nature*, *299*(5885), 715–717. https://doi.org/10.1038/299715a0

Nesbitt, H. W., & Young, G. M. (1989). Formation and diagenesis of weathering profiles. *The Journal of Geology*, *97*(2), 129–147. https://doi.org/10.1086/629290

Noffke, N. (2010). *Geobiology: Microbial mats in sandy deposits from the Archean Era to today*. Springer.

Nordt, L. C., & Driese, S. D. (2010). New weathering index improves paleorainfall estimates from Vertisols. *Geology*, *38*(5), 407–410. https://doi.org/10.1130/G30689.1

Novoselov, A. A., & de Souza Filho, C. R. (2015). Potassium metasomatism of Precambrian paleosols. *Precambrian Research*, *262*, 67–83. https://doi.org/10.1016/j.precamres.2015.02.024

Olawsky, K. J., & Kofod, F. (2019). *Miriwoong Woorlang Yawoorroonga-Woor*. Mirima Dawang Woorlab-garring Language and Cultural Center.

Öpik, A. A. (1970). *Redlichia* of the Ordian (Cambrian) of Northern Australia and New South Wales. *Bulletin of the Bureau of Mineral Resources Geology and Geophysics Canberra*, *114*, 1–66.

Óskarsson, B. V., Riishuus, M. S., & Arnalds, Ó. (2012). Climate-dependent chemical weathering of volcanic soils in Iceland. *Geoderma*, *189-190*, 635–651. https://doi.org/10.1016/j.geoderma.2012.05.030

Parcha, S. K., & Pandey, S. (2011). Ichnofossils and their significance in the Cambrian successions of the Parahio Valley in the Spiti Basin, Tethys Himalaya, India. *Journal of Asian Earth Sciences*, *42*(6), 1097–1116. https://doi.org/10.1016/j.jseaes.2011.04.028

Peckmann, J., Goedert, J. L., Thiel, V., Michaelis, W., & Reitner, J. (2002). A comprehensive approach to the study of methane-seep deposits from the Lincoln Creek Formation, western Washington State, USA. *Sedimentology*, *49*(4), 855–873. https://doi.org/10.1046/j.1365-3091.2002.00474.x

Plumb, K. A., Derrick, G. M., Needham, R. S., & Shaw, R. D. (1981). The Proterozoic of northern Australia. In. D. R. Hunter (Ed.), *Precambrian of the southern hemisphere*. (pp. 205–307, Vol. 2). Elsevier.

Prave, A. R. (2002). Life on land in the Proterozoic: Evidence from the Torridonian rocks of northwest Scotland. *Geology*, *30*(9), 811–814. https://doi.org/10.1130/0091-7613(2002)0300811:LOLITP2.0.CO;2

Pu, J. P., Bowring, S. A., Ramezani, J., Myrow, P., Raub, T. D., Landing, E., Mills, A., Hodgin, E., & Macdonald, F. A. (2016). Dodging snowballs: Geochronology of the Gaskiers glaciation and the first appearance of the Ediacaran biota. *Geology*, *44*(11), 955–958. https://doi.org/10.1130/G38284.1

Ramakrishnan, D., & Tiwari, K. C. (1999). REE chemistry of arid zone calcrete profiles–A case study from the Thar Desert. *India. Turkish Journal of Earth Sciences*, *7*(2), 97–104. https://journals.tubitak.gov.tr/earth/abstract.htm?id=2002

Rawling, J. E. (2000). A review of lamellae. *Geomorphology*, *35*(1–2), 1–9. https://doi.org/10.1016/S0169-555X(00)00015-5

Renaut, R. W., & Tiecerlin, J-J. (1994). Lake Bogoria, Kenya Rift Valley – a sedimentological overview. In R. W. Renaut & W. M. Last (Eds.), *Sedimentology and Geochemistry of Modern and Ancient Saline Lakes* (pp. 101–124, Vol. 50). Society for Sedimentary Geology Special Publication.

Retallack, G. J. (1976). Triassic palaeosols in the upper Narrabeen Group of New South Wales. Part I: Features of the palaeosols. *Journal of the Geological Society of Australia*, *23*(4), 383–399. https://doi.org/10.1080/00167617608728953

Retallack, G. J. (1991a). Untangling the effects of burial alteration and ancient soil formation. *Annual Review of Earth and Planetary Sciences*, *19*(1), 183–206. https://doi.org/10.1146/annurev.ea.19.050191.001151

Retallack, G. J. (1991b). *Miocene paleosols and ape habitats of Pakistan and Kenya*. Oxford University Press.

Retallack, G. J. (2005). Pedogenic carbonate proxies for amount and seasonality of precipitation in paleosols. *Geology*, *33*(4), 333–336. https://doi.org/10.1130/G21263.1

Retallack, G. J. (2008). Cambrian paleosols and landscapes of South Australia. *Australian Journal of Earth Sciences*, *55*(8), 1083–1106. https://doi.org/10.1080/08120090802266568

Retallack, G. J. (2011). Neoproterozoic loess and limits to Snowball Earth. *Journal of the Geological Society of London*, *168*(2), 289–308. https://doi.org/10.1144/0016-76492010-051

Retallack, G. J. (2012a). Criteria for distinguishing microbial mats and earths. In N. Noffke & H. Chafetz (Eds.), *Microbial mats in siliciclastic sediments* (pp. 136–152). *Society of Economic Paleontologists and Mineralogists Special Paper*. *101*.

Retallack, G. J. (2012b). Mallee model for mammal communities of the early Cenozoic and Mesozoic. *Palaeogeography, Palaeoclimatology, Palaeoecology*, *342-343*, 111–129. https://doi.org/10.1016/j.palaeo.2012.05.009

Retallack, G. J. (2013). Ediacaran life on land. *Nature*, *493*(7430), 89–92. https://doi.org/10.1038/nature11777

Retallack, G. J. (2014). Affirming life aquatic for the Ediacara biota in China and Australia: COMMENT. *Geology*, *42*(3), e325–e325. https://doi.org/10.1130/G35030C.1

Retallack, G. J. (2015a). Silurian vegetation stature and density inferred from fossil soils and plants in Pennsylvania, U.S.A. *Journal of the Geological Society London*, *172*(6), 693–709. https://doi.org/10.1144/jgs2015-022

Retallack, G. J. (2015b). Late Ordovician glaciation initiated by early land plant evolution, and punctuated by greenhouse mass-extinctions. *The Journal of Geology*, *123*(6), 509–538. https://doi.org/10.1086/683663

Retallack, G. J. (2016). Field and laboratory tests for recognition of Ediacaran paleosols. *Gondwana Research*, *36*, 107–110. https://doi.org/10.1016/j.gr.2016.05.001

Retallack, G. J. (2018). Oldest recognized paleosols on Earth, Panorama Formation (3.46 Ga), Western Australia. *Palaeogeography Palaeoclimatology Palaeoecology*, *489*, 230–248. https://doi.org/10.1016/j.palaeo.2017.10.013

Retallack, G. J. (2019). Interflag sandstone laminae, a novel fluvial sedimentary structure with implication for Ediacaran

paleoenvironments. *Sedimentary Geology*, *379*, 60–76. https://doi.org/10.1016/j.sedgeo.2018.11.003

Retallack, G. J. (2020). Boron paleosalinity proxy for deeply buried Paleozoic and Ediacaran fossils. *Palaeogeography Palaeoclimatology Palaeoecology*, *540*, 109536. https://doi.org/10.1016/j.palaeo.2019.109536

Retallack, G. J., & Broz, A. P. (2020). *Arumberia* and other Ediacaran–Cambrian fossils of central Australia. *Historical Biology*. https://doi.org/10.1080/08912963.2020.175581.

Retallack, G. J., & Huang, C. (2010). Depth to gypsic horizon as a proxy for paleoprecipitation in paleosols of sedimentary environments. *Geology*, *38*(5), 403–406. https://doi.org/10.1130/G30514.1

Retallack, G. J., Krinsley, D. H., Fischer, R., Razink, J. J., & Langworthy, K. A. (2016). Archean coastal-plain paleosols and life on land. *Gondwana Research*, *40*, 1–20. https://doi.org/10.1016/j.gr.2016.08.003

Retallack, G. J., & Mao, X. (2019). Paleoproterozoic (ca. 1.9 Ga) megascopic life on land in Western Australia. *Palaeogeography, Palaeoclimatology, Palaeoecology*, *532*, 109266. https://doi.org/10.1016/j.palaeo.2019.109266

Retallack, G. J., Marconato, A., Osterhout, J. T., Watts, K. E., & Bindeman, I. N. (2014). Revised Wonoka isotopic anomaly in South Australia and Late Ediacaran mass extinction. *Journal of the Geological Society of London*, *171*(5), 709–722. https://doi.org/10.1144/jgs2014-016

Retallack, G. J., & Mindszenty, A. (1994). Well preserved Late Precambrian paleosols from northwest Scotland. *Journal of Sedimentary Research*, *A64*(2), 264–281. https://doi.org/10.1306/D4267D7A-2B26-11D7-8648000102C1865D

Ruhe, R. V., & Olson, C. G. (1980). Clay mineral indicators of glacial and non-glacial sources of Wisconsinan loesses in southern Indiana, USA. *Geoderma*, *24*(4), 283–297. https://doi.org/10.1016/0016-7061(80)90056-7

Runnegar, B. (1995). Vendobionta or metazoa? Developments in understanding the Ediacara ''fauna. *Neues Jahrbuch Für Geologie Und Paläontologie—Abhandlungen*, *195*(1–3), 303–318. https://doi.org/10.1127/njgpa/195/1995/303

Sadek, S., Rabih, S., & Lagzi, I. (2010). Liesegang patterns in nature: A diverse scenery across the sciences. *Precipitation Patterns in Reaction-Diffusion Systems*, *661*, 1–43.

Schulz, M., Stonestrom, D., Lawrence, C., Bullen, T., Fitzpatrick, J., Kyker-Snowman, E., Manning, J., & Mnich, M. (2016). Structured heterogeneity in a marine terrace chronosequence: Upland mottling. *Vadose Zone Journal*, *15*(2), vzj2015.07.0102. https://doi.org/10.2136/vz/2015.07.0102 https://doi.org/10.2136/vzj2015.07.0102

Scotese, C. R. (2009). Late Proterozoic plate tectonics and palaeogeography: A tale of two supercontinents, Rodinia and Pannotia. In J. Craig, J. Thurow, B. Thusu, A. Whitham & Y. Abutarruma (Eds.), *Global Neoproterozoic Petroleum Systems: The Emerging Potential in North Africa* (pp. 67–83). Geological Society of London, Special Publication, 326. https://doi.org/10.1144/SP326.4

Seilacher, A., Grazhdankin, D., & Legouta, A. (2003). Ediacaran biota: The dawn of animal life in the shadow of giant protists. *Paleontological Research*, *7*(1), 43–54. https://doi.org/10.2517/prpsj.7.43

Setti, M., Marinoni, L., & Lopez-Galindo, A. (2004). Mineralogical and geochemical characteristics (major, minor, trace elements and REE) of detrital and authigenic clay minerals in a Cenozoic sequence from Ross Sea. *Clay Minerals*, *39*(4), 405–421. https://doi.org/10.1180/000985503540143

Sheldon, N. D. (2003). Pedogenesis and geochemical alteration of the Picture Gorge subgroup, Columbia River basalt, Oregon. *Geological Society of America Bulletin*, *115*(11), 1377–1387. https://doi.org/10.1130/B25223.1

Sheldon, N. D., & Retallack, G. J. (2001). Equation for compaction of paleosols due to burial. *Geology*, *29*(3), 247–250. https://doi.org/10.1130/0091-7613(2001)0290247:EFCOPD2.0.CO;2

Sheldon, N. D., Retallack, G. J., & Tanaka, S. (2002). Geochemical climofunctions from North American soils and application to paleosols across the Eocene–Oligocene boundary in Oregon. *The Journal of Geology*, *110*(6), 687–696. https://doi.org/10.1086/342865

Shen, B., Xiao, S., Zhou, C., & Yuan, X. (2009). *Yangtziramulus zhangi* new genus and species, a carbonate-hosted macrofossil from the Ediacaran Dengying Formation in the Yangtze Gorges area. *Journal of Paleontology*, *83*(4), 575–587. https://doi.org/10.1666/08-042R1.1

Soil Survey Staff. (2014). *Keys to soil taxonomy*. Natural Resources Conservation Service.

Sprigg, R. C. (1949). Early Cambrian "jellyfishes" at Ediacara, South Australia and Mount John, Kimberley District, Western Australia. *Transactions of the Royal Society of South Australia*, *73*(1), 72–99.

Stace, H. C. T., Hubble, G. D., Brewer, R., Northcote, K. H., Sleeman, J. R., Mulcahy, M. J., & Hallsworth, E. G. (1968). *A handbook of Australian soils*. Rellim.

Stimson, M. R., Miller, R. F., MacRae, R. A., & Hinds, S. J. (2017). An ichnotaxonomic approach to wrinkled microbially induced sedimentary structures. *Ichnos*, *24*(4), 291–316. https://doi.org/10.1080/10420940.2017.1294590

Sugahara, H., Sugitani, K., Mimura, K., Yamashita, F., & Yamamoto, K. (2010). A systematic rare-earth elements and yttrium study of Archean cherts at the Mount Goldsworthy greenstone belt in the Pilbara Craton: Implications for the origin of microfossil-bearing black cherts. *Precambrian Research*, *177*(1–2), 73–87. https://doi.org/10.1016/j.precamres.2009.10.005

Surge, D. M., Savarese, M., Dodd, J. R., & Lohmann, K. C. (1997). Carbon isotopic evidence for photosynthesis in Early Cambrian oceans. *Geology*, *25*(6), 503–506. https://doi.org/10.1130/0091-7613(1997)0250503:CIEFPI2.3.CO;2

Sweet, I. P., Mendum, J. R., Morgan, C. M., & Pontifex, I. R. (1974). *The geology of the Northern Victoria River Region, NT*. Bureau of Mineral Resources Geology and Geophysics Report (Vol. 166). Bureau of Mineral Resources Geology and Geophysics. https://ecat.ga.gov.au/geonetwork/srv/eng/catalog.search#/metadata/15078

Sweet, I. P., Pontifex, I. R., & Morgan, C. M. (1974). *Geology of the Auvergne 1:250 000 Sheet Area, NT (excluding Bonaparte Gulf Basin)*. Bureau of Mineral Resources Geology and Geophysics Report (Vol. 161). Bureau of Mineral Resources Geology and Geophysics. https://ecat.ga.gov.au/geonetwork/srv/eng/catalog.search#/metadata/15076

Talbot, M. R. (1990). A review of the palaeohydrological interpretation of carbon and oxygen isotopic ratios in primary lacustrine carbonates. *Chemical Geology: Isotope Geoscience Section*, *80*(4), 261–279. https://doi.org/10.1016/0168-9622(90)90009-2

Taylor, R. S., Hawco, J. B., Nichols, R., & McIlroy, D. (2019). A critical reappraisal of the holotype of *Beothukis mistakensis*, a unique exceptionally preserved rangeomorph organism from Mistaken Point, Newfoundland, Canada. *Estudios Geológicos*, *75*(2), e117. https://doi.org/10.3989/egeol.43586.572

Terry, R. D., & Chilingar, G. V. (1955). Summary of "Concerning some additional aids in studying sedimentary formations," by MS Shvetsov. *Journal of Sedimentary Research*, *25*(3), 229–234. https://doi.org/10.1306/74D70466-2B21-11D7-8648000102C1865D

Trainer, D. W. (1931). Zebra Rock. *American Mineralogist*, *16*, 221–225.

Ufnar, D. F., Gröcke, D. R., & Beddows, P. A. (2008). Assessing pedogenic calcite stable-isotope values: Can positive linear covariant trends be used to quantify palaeo-evaporation rates?. *Chemical Geology*, *256*(1–2), 46–51. https://doi.org/10.1016/j.chemgeo.2008.07.022

Veizer, J., Ala, D., Azmy, K., Bruckschen, P., Buhl, D., Bruhn, F., Carden, G. A. F., Diener, A., Ebneth, S., Godderis, Y., Jasper, T., Korte, C., Pawellek, F., Podlaha, O. G., & Strauss, H. (1999). $^{87}Sr/^{86}Sr$, $\delta^{13}C$ and $\delta^{18}O$ evolution of Phanerozoic seawater. *Chemical Geology*, *161*(1–3), 59–88. https://doi.org/10.1016/S0009-2541(99)00081-9

Vepraskas, M. J., & Sprecher, S. W. (1997). Summary. In M. J. Vepraskas & S. W. Sprecher (Eds.), *Aquic conditions and hydric soils: The problem soils* (pp. 153–156). Soil Science Society of America Special Publication 150.

Wallace, M. W., & Hood, A. S. (2018). Zebra textures in carbonate rocks: Fractures produced by the force of crystallization during mineral replacement. *Sedimentary Geology*, *368*, 58–67. https://doi.org/10.1016/j.sedgeo.2018.03.009

Walter, M. R. (1976). *Stromatolites*. Elsevier.

Wan, B., Chen, Z., Yuan, X., Pang, K., Tang, Q., Guan, C., Wang, X., Pandey, S. K., Droser, M. L., & Xiao, S. (2020). A tale of three taphonomic modes: The Ediacaran fossil *Flabellophyton* preserved in limestone, black shale, and sandstone. *Gondwana Research*, *84*, 296–314. https://doi.org/10.1016/j.gr.2020.04.003

Weinberger, R. (2001). Evolution of polygonal patterns in stratified mud during desiccation: The role of flaw distribution and layer boundaries. *Geological Society of America Bulletin*, *113*(1), 20–31.https://doi.org/10.1130/0016-7606(2001)1130020:EOPPIS2.0.CO;2

Williams, G. E., Gostin, V. A., McKirdy, D. M., & Preiss, W. V. (2008). The Elatina glaciation, late Cryogenian (Marinoan Epoch), South Australia: Sedimentary facies and palaeoenvironments. *Precambrian Research*, *163*(3–4), 307–331. https://doi.org/10.1016/j.precamres.2007.12.001

Winchester, J. A., & Floyd, P. A. (1977). Geochemical discrimination of different magma series and their differentiation products using immobile elements. *Chemical Geology*, *20*, 325–343. https://doi.org/10.1016/0009-2541(77)90057-2

Ziegenbalg, S. B., Brunner, B., Rouchy, J. M., Birgel, D., Pierre, C., Böttcher, M. E., Caruso, A., Immenhauser, A., & Peckmann, J. (2010). Formation of secondary carbonates and native sulphur in sulphate-rich Messinian strata, Sicily. *Sedimentary Geology*, *227*(1–4), 37–50. https://doi.org/10.1016/j.sedgeo.2010.03.007